UNIVERSIDADE DE LISBOA
FACULDADE DE CIÊNCIAS
DEPARTAMENTO DE BIOLOGIA ANIMAL

# Regeneration Dynamics of the Radial Nerve Cord in the Sea Star *Marthasterias glacialis (Linnaeus, 1758)*

Filipe Teixeira dos Reis Peixoto de Magalhães

**Mestrado em Biologia Humana e Ambiente**

Dissertação orientada por:
Doutora Ana Varela Coelho
Prof. Doutora Rita Zilhão

2021

# ACKNOWLEDGMENTS

*Because all the people who have helped me throughout the progress of my master thesis have played an active role. Thank you very much for the fellowship, motivation and the help that allowed me to enjoy this wonderful experience.*

Um agradecimento especial à professora Dra. Ana Varela Coelho. Obrigado, Ana, por ter feito de mim melhor trabalhador, investigador e sobretudo aluno da ciência. Por ter tido a exigência quando as circunstâncias assim o exigiam e ter retirado de mim o meu melhor. Pela orientação, ajuda e disponibilidade constante. Por ter feito de mim uma pessoa substancialmente mais rica em conhecimento do que aquela que iniciou este trabalho. Muito obrigado por ter permitido a minha participação neste projeto e que o futuro seja risonho para todas as pessoas que irão dar a sua contribuição. Não poderia também deixar de elogiar o ITQB Nova pelas fantásticas instalações que proporcionaram, na medida do possível, todas as condições para a realização do trabalho experimental. Obrigado ao Dr. Laidson Gomes e à minha colega Ana Filipa Fernandes pela ajuda e pelos ensinamentos na quantificação das proteínas. Obrigado ao Dr. Luís Gafeira pela assistência no tratamento e discussão dos resultados científicos. Obrigado aos meus colegas Cassandra Santos e Tomás Ochoa pela preciosa ajuda na recolha das estrelas-do-mar.

Agradeço à Faculdade de Ciências, e a todos os seus responsáveis. Agradeço à professora Dra. Rita Zilhão pela orientação burocrática, pelas sugestões e pela ajuda fundamental na realização da escrita desta dissertação. A todos os professores do mestrado de Biologia Humana e Ambiente, que me providenciaram mais conhecimento científico ao longo de um ano árduo de ensino, muito obrigado.

Agradeço à Dra. Claúdia Andrade pela fantástica realização e ajuda no procedimento de citometria de fluxo e ao CEDOC pela permissão de utilização dos seus equipamentos. Agradeço também ao Dr. José Rino pelos ensinamentos de citometria de fluxo de imagem e do software IDEAS.

Um agradecimento aos responsáveis do Aquário Vasco da Gama por apostarem na investigação sobre os invertebrados marinhos da nossa costa portuguesa e por terem permitido a utilização das suas instalações sempre que precisei. Obrigado ao senhor Miguel pela colaboração na manutenção das estrelas-do-mar e ter disponibilizado o seu local de trabalho para a realização dos ensaios experimentais.

Por fim, um agradecimento à COST Action pela minha realização do short-term scientific mission em Itália, que me permitiu conhecer novos métodos experimentais, metodologias de trabalho e uma nova cultura, uma experiência extremamente enriquecedora. Dra. Michela Sugni, grazie mille per avermi permesso di andare a Milano, per la tua guida nelle procedure istologiche e per aver trasmesso la conoscenza. Ringrazio anche i miei colleghi dall'Italia, Giulia Driussi e Giulia Pria per la loro collaborazione e insegnamenti nelle procedure istologiche (sorry for my bad Italian!!).

# TABLE OF CONTENTS

# RESUMO ALARGADO

A regeneração é um processo conservativo de desenvolvimento pós-embrionário que ocorre nas células somáticas e sucede em indivíduos no estado larval, jovens e adultos. Envolve a reparação e reposição de células, tecidos e órgãos, ou até mesmo a substituição de partes corporais inteiras com a mesma estrutura, forma e polaridade. Este mecanismo é despoletado após uma lesão traumática ou amputação devido a predação, ou quando o próprio organismo realiza autotomia como mecanismo de defesa à predação ou como mecanismo de reprodução assexuada. No entanto, a capacidade de regeneração é diversa para as várias espécies. Em particular, os mamíferos apresentam uma ineficiente regeneração ao nível do Sistema Nervoso Central (SNC) após lesão traumática, o que resulta na perda ou deficiências de atividade motora. Por outro lado, a regeneração do SNC, assim como a regeneração de outros tecidos, órgãos e membros corporais, tem elevada expressão nos equinodermes. Tornando-se por isso, fundamental estudar o processo de regeneração nos equinodermes, com o objetivo de compreender a evolução e os mecanismos do SNC nos humanos, assim como perceber as causas deste processo não estar ativo em certos sistemas anatómicos, apresentando-se as estrelas-do-mar como relevante modelo de estudo. Nestes organismos a regeneração pós-traumática e pós-autotomia do braço tem sido recorrentemente alvo de investigação, ao passo que a regeneração do SNC não tem colhido tanto interesse pela comunidade científica. Por estes motivos, este projeto destinou-se a estudar a fase inicial do processo de regeneração pós-traumática do Cordão Nervoso Radial (RNC) da estrela-do-mar da espécie *Marthasterias glacialis*. Esta espécie, denominada comumente como estrela-do-mar de espinhos derivado do seu corpo ser coberto por espinhos, detém de uma extraordinária capacidade para regenerar partes do corpo, possui o RNC numa posição anatómica exterior e apresenta uma elevada abundância nas praias da costa portuguesa, sendo por isso largamente utilizada como organismo modelo nos estudos de regeneração. Desta forma, com o objetivo de investigar os processos celulares e moleculares que lhe estão associados foi estudada a histologia do tecido nervoso em regeneração e as dinâmicas das populações celulares e das proteínas circulantes no fluído celómico. O processo regenerativo desencadeado pela amputação de uma porção do RNC na parte distal da ponta do braço da estrela-do-mar foi estudado em três pontos-temporais (1 dia, 7 dias e 14 dias após excisão parcial do nervo). Relativamente ao estudo das proteínas solubilizadas no fluído celómico livre de células (CFF), foi efetuada a sua quantificação total pelo método espectrofotométrico de BCA depois de removida a porção celular do fluído celómico (celomócitos). Verificaram-se diferenças significativas na quantidade de proteína total no CFF entre o dia 1 pós-amputação do nervo (p.a.) e o dia 14 p.a., e entre todos os pontos temporais e o grupo controlo. No entanto, foram também encontradas diferenças significativas em amostras de CFF de animais controlo recolhidas em dias diferentes. O que implicará a realização de novos ensaios usando grupos controlo para cada dia de recolha de fluído coelómico. Para o estudo das populações celulares circulantes no fluído celómico, foi usada marcação com DRAQ5 de forma a caracterizar as células vivas, e obter valores de *side scatter*, *forward scatter*, incorporação de DRAQ5 e determinar a percentagem de eventos celulares por citometria de fluxo (CF). Com base em ensaios de CF tinham sido descritas em Andrade et al. (2021), duas populações celulares em animais não amputados (P1 e P2). P2 apresentou valores de incorporação de DRAQ5 e de *side scatter* superiores aos valores medidos para P1. As mesmas duas populações foram observadas no grupo controlo usado neste estudo. Verificou-se que as percentagens de eventos celulares para estas duas populações não apresentam diferenças significativas durante o processo de regeneração. No entanto, destaca-se a observação de uma nova população de celomócitos, aqui designada P3. Esta população surge na maioria das amostras a partir do dia 7 p.a. e ganha maior evidência no dia 14 p.a. Em concordância, foram registadas diferenças significativas na sua abundância entre o grupo controlo e os dias 7 e 14 p.a, e entre

o dia 1 p.a e os dias 7 e 14 p.a. Esta população celular (P3) apresenta valores de *side scatter* que podem ser associados à medição da sua complexidade morfológica, similares aos das células da população P1. Enquanto os níveis de incorporação de DRAQ5 da população P3 são similares aos da população P2. O estudo morfológico dos padrões tecidulares e celulares do nervo em regeneração foi efetuado através de técnicas histológicas, com recurso ao método de coloração tricromática e visualização dos tecidos por microscopia ótica. Nesta análise evidencia-se uma rápida regeneração do tecido nervoso amputado e uma mudança gradual na sua conformação ao longo do tempo de regeneração. No dia 1 p.a ainda não é possível visualizar a reposição da ligação do cordão nervoso no local onde ocorreu a sua excisão parcial. No dia 7 p.a. já é possível verificar a existência de tecido nervoso a ligar as duas extremidades lesionadas, porém com reduzida espessura, especialmente na zona do neuropilo. No dia 14 p.a este tecido em regeneração apresenta maior espessura com dimensões e estrutura semelhantes ao tecido original. Com a particularidade de presumivelmente a zona somática do epitélio ectoneural, que é constituída pelos corpos celulares dos neurónios e das células gliais radiais, ser a primeira a ser regenerada, só depois seguida pela zona do neuropilo. Em concordância com o processo morfaláctico, verifica-se ainda hipertrofia do seio hiponeural, do canal vascular aquífero e do canal hemal, possivelmente em consequência do fluxo de fatores moleculares e/ou a migração de células que poderão coadjuvar no processo regenerativo. Adicionalmente, também é possível visualizar nos três pontos-temporais a retração dos pés ambulacrários na região de amputação do nervo, presumivelmente como mecanismo comportamental de defesa e de proteção da região lesionada.

Previamente à realização dos ensaios acima descritos, e com o propósito de controlar a variabilidade biológica encontrada em estudos anteriores, avaliou-se um conjunto de parâmetros de fácil determinação sem recurso a processos invasivos que permitissem distinguir entre machos e fêmeas. A sua futura utilização iria permitir separar os animais em função do género e, consequentemente a realização dos ensaios de regeneração para cada um dos géneros, anulando a eventual contribuição deste fator nestes estudos. De modo a cumprir este objetivo, as estrelas-do-mar foram caracterizadas através de medidas biométricas tais como, o diâmetro do disco central, o peso, o comprimento e a largura dos braços, assim como as razões entre cada uma destas medidas. Foi ainda determinada a quantidade total de proteína no CFF e avaliada a sua correlação com as medidas biométricas. Concluiu-se que estes parâmetros não permitem criar um modelo preditivo do sexo de novos espécimes, não tendo sido possível fazer a separação dos animais em função do género nos ensaios de regeneração descritos. Apesar de não ter sido possível concluir sobre a influência do sexo na regeneração devido ao reduzido poder estatístico, os resultados obtidos não sugerem que esta seja a causa das diferenças encontradas nestes estudos.

Por fim, foi também realizada a distinção com base em parâmetros morfológicos e pelas determinações efetuadas por citometria de fluxo de imagem (CFI) das subpopulações de celomócitos de cada uma das duas populações anteriormente caracterizadas em Andrade *et al*. (2021). As imagens obtidas por CFI foram associadas a três subpopulações da população P1, uma subpopulação a mais do que tinha sido caracterizado anteriormente, e aqui designada como P1B, e a 4 subpopulações da população P2. Cada par de subpopulações entre cada população foi sujeito a um algoritmo de inteligência artificial, a partir do qual obteve-se os parâmetros que permitem uma melhor discriminação. Onde, consequentemente, foi possível obter uma boa distinção entre cada par das três subpopulações da P1 através de parâmetros de textura, e das quatro subpopulações da P4 em termos de textura, forma ou tamanho celular. Estes parâmetros serão usados em futuros estudos das dinâmicas das células circulantes após a indução de regeneração.

**Palavras-chave:** regeneração pós-traumática do cordão nervoso radial, fluído celómico, celomócitos, quantidade total de proteína.

# ABSTRACT

Mammals show inefficient regeneration at the level of the Central Nervous System (CNS) posteriorly to the traumatic lesion, which results in loss or disabilities of motor activity. However, the regeneration of the CNS in deuterostomes has its maximum expression in echinoderms. Therefore, it is essential to study the regenerative process in echinoderms to understand their differential mechanisms in humans. This project aimed to study the post-traumatic Radial Nerve Cord (RNC) regeneration of the starfish *Marthasterias glacialis* at 1, 7, and 14 days after partial nerve excision, through the characterization of the coelomic fluid cellular populations (coelomocytes) by flow cytometry (FC), the cellular processes and patterns of the nerve tissue through histology tools and the determination of the total protein in the cell-free celomic fluid (CFF). A new population of coelomocytes was identified by FC at 7 days post-amputation (p.a.) and its presence reinforcement at 14 days p.a., suggesting its involvement in the regeneration process. Histological analysis showed a rapid regeneration of the amputated nervous tissue, resembling the non-regenerating tissue at 14 p.a. On day 7 p.a. the RNC injured ends are connected by nerve tissue consisting of the hyaline layer, the somatic zone, and the hyponeural epithelia, although with a neuropile thin layer. Additionally, a hypertrophy of the coelomic canals is accentuated proposing an increment of molecules and/or cells migration. In accordance, CFF total protein shows an augmentation trend from day 1 to 14 p.a. To reduce eventual biological variability due to gender a biometric study was performed. It was concluded that M. glacialis specimens do not have external sexual dimorphism hampering a regeneration study specific for each gender. Finally, a distinction between coelomocytes subpopulations was successfully made based on optical and morphological parameters by image flow cytometry (IFC) through an artificially intelligence algorithm.

**Keywords:** post-traumatic radial nerve cord regeneration, coelomic fluid, coelomocytes, total quantity of proteins.

# LIST OF FIGURES

**Figure 3.2.1.** Differentiation between P1S **(A)** and P1L **(B)** cells trough the texture parameters of background mean and bright detail intensity **(C). A** and **B** are representations of images or signals detected by side scatters (channels 1 and 6), bright field (channel 1 and 9), FM 4-64 marker (channel 5), and DAPI (channel 7). Yellow diamond- P1L; purple triangle- P1S.

**Figure 3.2.2.** Differentiation between P1B (**A**), with P1S (**B**) and P1L (**C**) cells trough the texture parameters of modulation and standard deviation object**. A** is a representation of images or signals detected by side scatters (channels 1 and 6), bright field (channel 1 and 9), FM 4-64 marker (channel 5), and DAPI (channel 7). Yellow diamod- P1L; green square- P1N; purple triangle- P1S.

**Figure 3.2.3.** Representation of images or signals of petaloid (**A**), filopodial (**B**), big granulated (**C**), and polygonal (**D**) cells, detected by side scatters (channels 1 and 6), bright field (channel 1 and 9), FM 4-64 marker (channel 5), and DAPI (channel 7).

**Figure 3.2.4.** Differentiation between petaloid and filopodial cells (**A**), big granulated with polygonal cells (**B**), petaloid with polygonal (**C**), and big granulated cells (**D**), filopodial with polygonal (**E**), and big granulated cells (**F**), through the texture features of modulation and standard deviation object, the size features of cell area and height, and the shape features of circularity of the object, thickness, and shape ratio. Yellow diamond- petaloid; green square- filopodial; blue empty circle- big granulated; purple cross- polygonal.

**Figure 3.3.1.** Mean concentration of proteins circulating in the coelomic fluid free of cells in the homeostatic state (control group) and at the regeneration times: 1, 7 and 14 days. N= 10 (control group), 6 (day 1), 4 (day7) and 5 (day 14). The mean concentration for the control group was determined for the total control animals, independently of the day. Note: * means p-value<0.05; ** means p-value<0.01.

**Figure 3.3.2.** Quantification of proteins circulating in the coelomic fluid free of cells of control animals in two different days: 24/mar and 31/mar. N= 18 (8 in 24/mar and 10 in 31/mar). Note: * means p-value<0,05.

**Figure 3.3.3.** Flow cytometry analysis of a typical dot plot of circulating coelomocytes stained with DRAQ5 of 6 non-regenerating individuals.

**Figure 3.3.4.** P2 coelomocyte morphotype detected by fluorescence microscopy in the CF of *M. glacialis*. Adapted from [45].

**Figure 3.3.5.** Coelomocytes flow cytometry analysis during Radial Nerve Cord (RNC) regenerative process. Typical dot plots of circulating coelomocytes stained with DRAQ5 at days 1, 7 and 14 after partial nerve excision. N=5 per time-point.

**Figure 3.3.6.** Bar plots of the mean proportion of P1 (**A**), P2 (**B**) and new P3 (**C**) cells in control and in each time-point (1, 7 and 14 days) of the radial nerve regeneration. N=21 (6 controls and 5 in each time-point). Note: * means p-value<0,05.

**Figure 3.3.7.** Proximal section at the sagittal plane of a non-regenerative sea star *M. glacialis*. Orientation: **P**- proximal; **D**- distal; **Ab**- aboral side; **Or**- oral side. Identification: **AO**- ambulacral ossicle; **CC**- coelomic cavity; **CE**- coelomic epithelium; **D**- dermis; **Ep**- epidermis; **HS**- hyponeural sinus; **Pe**- pedicellariae; **RNC**- radial nerve cord; **Sp**- spine; **TF**- tube foot; **TLM**- transversal lower muscle; **TUM**- transversal upper muscle.

**Figure 3.3.8.** Section of the radial nerve cord (RNC), which is composed by: **Hn**- hyponeural; **Cn**- connective tissue; **En**- ectoneural, which is formed by: **N**- neuropile; **S**- somatic zone (cell body layer); and **Hi**- hyaline layer. Orientation: **Ab**- aboral side; **Or**- oral side.

**Figure 3.3.9.** Transversal section of the regenerative arms from the period of regeneration of: (**A)** 1 day, (**B**) 7 days, (**C**) 14 days. Representation of the radial nerve cord: (arrows) the non-regenerative end, and (square) the gap/regenerative tissue.; **AO**- ambulacral ossicle; **CC**- coelomic cavity; **HS**- hyponeural sinus; **RWC**- radial water canal; **TF**- tube feet. Orientation: **Ab**- aboral side; **Or**- oral side.

**Figure 3.3.9.** Transversal sections amplified (40x) of the regenerative arms. (**A)** Section of the clump in day 1 post-traumatic amputation of the nerve. Sections of the RNC in regeneration at 7 days p.a. (**B**) and at 14 days (**C**), and non-regenerative RNC (**D**). **CE**- coelomic epithelium; **Cn**- connective tissue; **Hi**- hyaline layer; **Hn**- hyponeural zone; **HS**- hyponeural sinus; **N**- neuropile; **S**- somatic (cell body) zone. Orientation of the figures: proximal part in the left side to distal part on the right side; aboral side at upper limit and oral side at the lower limit.

# LIST OF TABLES

# LIST OF ABREVIATIONS

**Al**- arm length
**Aw**- arm width
**CDd-** central disk diameter
**CF**- coelomic fluid
**CFF**- coelomic fluid free of cells
**CNS**- central nervous system
**FC**- flow cytometry
**FSC**- forward scatter
**HS**- hyponeural sinus
**IFC**- image flow cytometry
**IS**- immune system
**MCT**- mutable collagenous tissue
**NS-** nervous system
**PNS**- peripheral nervous system
**RNC**- radial nerve cord
**RWC**- radial water canal
**SSC**- side scatter
**xAl**- mean arm length
**xAw**- mean arm width
**W**- weight
**WVC**- water-vascular canal
**WVS**- water vascular system

# 1. INTRODUCTION

## 1.1. Echinoderms

Echinodermata in Greek is defined by spiny ("*echino*") skin ("*dermata*"). Meaning that the organisms of this phylum, designated as echinoderms, are exclusively marine deuterostome invertebrates characterized by hard spiny skin. Being these characteristics the essence of echinoderms, consequently, they are divided into six extant classes: Asteroidea (sea stars), Concentricycloidea (sea daisies), Crinoidea (sea lilies and feather stars), Echinoidea (sea urchins), Ophiuroidea (brittle stars), and Holothuroidea (sea cucumbers) [1-2].

Echinodermata, alongside Hemichordata, takes part of the Ambulacria, a sister clade of the phylum Chordata, including vertebrates, and altogether belong to the superphylum Deuterostomia [3] (**Figure 1.1**). This close relationship offers an important reason to comprehend the machinery, physiology, and processes, of the echinoderm nervous system (NS), and to use them as models to understand the evolution of the chordate´s NS [1] and stem cells potential for regeneration, with possible applicability and transferability to biomedicine.

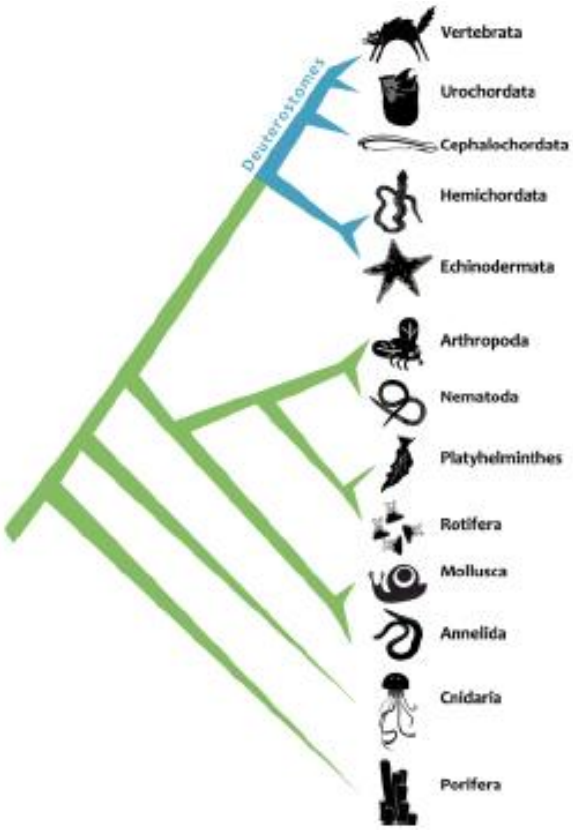


**Figure 1.1**. Phylogenetic tree demonstrating the relationship between Echinodermata and the other phyla. Adapted from [4].

# 1.2. Asteroids

Currently, one of the most important regeneration models and one of the most studied are the starfish, scientifically called asteroids. Asteroids are sessile animals with a star-like shape and an oral-aboral flattened body constituted by a central disk, from which radiates five or more arms, and with a very particular characteristic, the absence of an anterior cephalic structure [5].

Like all echinoderms, asteroids display as morphologic features: 1) a bilateral symmetry in larvae and a pentaradial body plan in adults; 2) a mesodermal calcitic endoskeleton; 3) a unique mutable collagenous tissue (MCT) controlled by the central nervous system (CNS) under situations of fission or autotomy; 4) and a unique hydraulic water-vascular system (WVS) involved in locomotion, feeding, respiration, and sensation [6].

Usually, the oral side of the organism features the mouth, situated in the middle of the central disk, connected to ambulacral grooves (correspondent to the number of the arms), with ambulacral feet (tube feet or podia) along the groove and optic cushions (photoreceptors) at the extremity. The aboral side harbors the anus, the madreporite (a respiratory structure), and the spines (defense structures) (**Figure 1.2.1**).

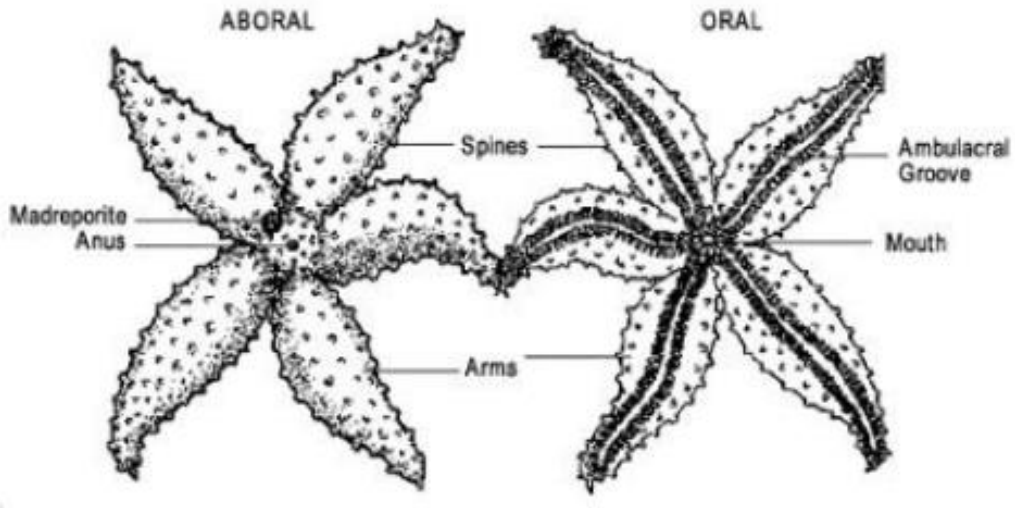


**Figure 1.2.1.** General external morphology of asteroids

Internally, the sea stars possess the skeletal, digestive, reproductive, nervous, water-vascular, and circulatory systems. Generally, these systems follow the radial pattern where several sets of major organs are centered in the disk and are branched into equal radial organs arranged around the aboral-oral axis in every single arm [7]. Meaning that each arm has a replica of all the internal organs (**Figure 1.2.2**).

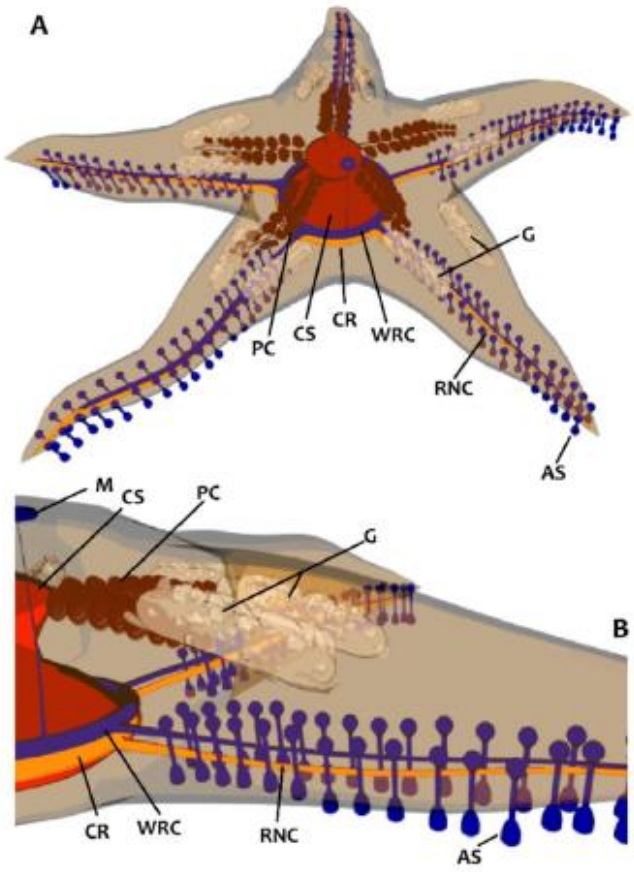


**Figure 1.2.2.** Internal morphology of an asteroid. (**A**) Top view and (**B**) lateral view of the sea star anatomy. The organ systems are centered in the central disk and radiated in each arm. Nervous system: CR, circumoral nerve ring; RNC, radial nerve cord. Digestive system: CS, cardiac stomach; PC, pyloric caeca. Water vascular system: WRC, water ring canal; AS, ambulacrary system with tube feet; M, madreporite. Reproductive system: G, gonads. Adapted from [4].

From a simple point of view, the structure of the sea star´s body is internally formed by the body wall and the body cavity. The body wall is segmented in the epidermis, dermis, and coelomic epithelium (CE), also called the peritoneum. The epidermis is formed by a single layer of cells and contains hairlike projections (cilia), skeletal elements (spines and pedicellariae), glandular and sensory cells. The dermis hosts the calcareous skeleton and connective tissues (MCT), and internally are outer circular and inner longitudinal muscle layers provided by the peritoneum [5,8]. The body cavity, also called coelom, is specialized into four regions: the perivisceral coelom, the axial sinus, the hyponeural sinus (HS), also designated as the perihaemal system, and the WVS. The perivisceral coelom is in contact with the peritoneum and is where the gonads and the digestive tube are suspended. The axial sinus belongs to the haemal system, which is composed of an axial organ and extended canals of haemal tissue located in the perihaemal coelom and is in contact with the HS [9]. This latter is an oral sinus with a longitudinal septum that forms in each arm the radial HS, situated above the radial nerve cord (RNC) [10] (**Figure 1.2.3**).

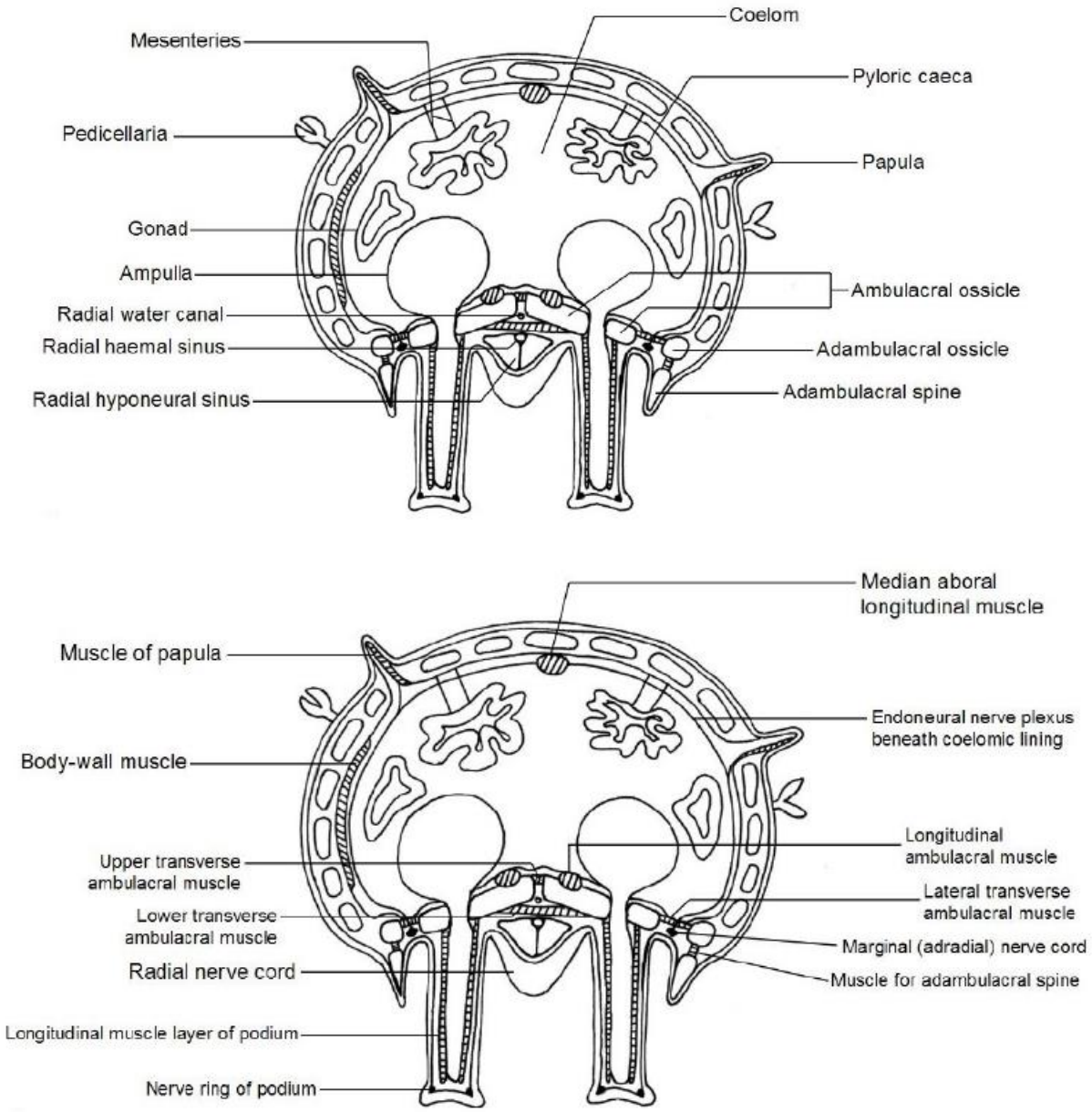


**Figure 1.2.3.** Transversal sections of the general anatomy of an asteroid´ arm. Upper scheme stands for the skeletal, digestive, and reproductive systems, and the coelomic cavities. Lower scheme stands for the nerve and muscular systems. Adapted from [10].

## Skeletal System

The skeletal system is dermal and is constituted by the exoskeleton and endoskeleton. The exoskeleton consists of calcareous appendages, such as spines and pedicellariae, on the surface of the body wall. The endoskeleton is composed by numerous separated and elongated or rounded plates of mineral calcium carbonates, called ossicles. Which are articulated with each other by a mesh of collagen fibers that gives space allowing the appearance of papullae (respiratory and excretory structures) in the aboral surface [5,8].

## Digestive System

The digestive system is composed of mouth, gut, small intestine, rectum, and anus. The gut occupies most of the disk and is extended to the arms, where is segmented in the cardiac stomach and pyloric stomach, with two extensions, called pyloric caeca [5].

## Reproductive System

Asteroids dispose of gonads as the only feature of the reproductive system. Most of the species are gonochoric, meaning that females own ovaries that produce eggs and males own testis that produces sperm [5].

## Nervous System

Even though sea stars possess a dispersed CNS without a centralized brain, the nervous system is so complex that can be subdivided into the peripheral nervous system (PNS) and CNS. The PNS is characterized by a sensory system in the epidermis and a motor system in the coating of the coelomic cavity, connected by neurons presented in the dermis [5]. The CNS is characterized by a circumoral nerve ring in the central disk that connects the RNCs of each arm running parallel to the radial canal [5-6]. This subsystem is connected to various parts of the body by peripheral motor nerves. For example, the RNCs extensively innervate several types of effectors, like the podia, muscles, peritoneum, epidermis, and numerous elements of the MCT, through metameric nerves [6]. Both nerve ring and RNC consist in an agglomeration of neurons and glial cells associated with an extensive neuropil. The RNC is organized in two adjacent parallel bands of neuroephitelia, a thicker outer ectoneural band, and a thinner inner hyponeural band, separated by a thin layer of connective tissue [11]. In terms of ratio, the RNC exhibit more radial glial cells than neurons [6]. The neurons are responsible for the electric signaling transmission between them and throughout the body [12]. However, identical to what occurs on the mammals' spinal cord, neurons in starfish may rely mainly on chemical synapses [13]. Their axons are small, not protected with myelin, and displayed in packages with a parallel arrangement. The glial cells are non-neuronal cells of the NS and are responsible for the support and homeostasis of the neurons [12].

## Water-Vascular System

The WVS consists of an internal hydraulic system that comprises the madreporite and a ring vessel connected by the stone canal (a calcified vessel) in the central disk. Additionally, five or more radial water canals (RWC), fluid-filled vessels, are extended from the ring vessel and give rise to the tube feet, which are in contact with the substrate and the seawater [5]. The ring vessel also contains bulbous cavities called Polian vesicles, which maintains the organism pressure and hold reserve supplies of coelomic fluid (CF).

## Immune System

The key piece of echinoderms immunity is the CF that circulates and fills in all the coelomic spaces of the body cavity, including the WVS, the perivisceral coelom, and the perihaemal system [12, 14-15]**.** This fluid, has a similar composition to seawater in term of minerals and have as its main function the circulation of the coelomic fluid cells, nutrients, metabolites, signaling, and defense molecules [16]. Essentially it is an extracellular body fluid homolog to human plasma, that baths the

internal organs, abundant in secreted molecules. In that manner, the immune system (IS) in echinoderms is efficient for host protection and operates with innate mechanisms in the absence of adaptive capability due to lack of memory [2]. Essentially, comprises two mechanisms, the humoral and the cellular immunity [17]. Humoral immunity consists of soluble factors, mostly secreted by the coelomic fluid cells (immune cells), such as lectins, agglutinins, lysins, antimicrobial peptides, and the prophenoloxidase (proPO) activating system, which act in parallel with the immune cells in antipathogenic responses [15,17]. Also, a great variety of molecules secreted by coelomocytes or surrounding tissues, like perforins and cytokines, can promote cell migration, agglutination, and healing [18]. The cell-mediated immunity is designed by the coelomic fluid cells, the effectors of defense reactions, such as clotting, phagocytosis, encapsulation, opsonization, and clamping, being able to recognize, neutralize, and consequently allow the clearance of pathogens and other foreign substances [2, 17-18].

## 1.3. Animal Model: *Marthasterias glacialis*

*Marthasterias glacialis* (Linnaeus, 1758) is a species of starfish of the class Asteroidea, known as spiny starfish since its body is made up of three rows of spines on each arm (**Figure 1.3.1**). It is a predatory species that exhibit a wide variety of population dynamics, occupies different types of habitats, from surface water to 200 m in-depth, and has a wide variety of colors and body sizes [19-21]. Are thought to not exhibit external sexual dimorphism and are known to resort only to sexual reproduction by external fertilization [20].

**Figure 1.3**. Sea star of the species *Marthasterias glacialis* collected in Praia da Poça (São João do Estoril, Lisboa).

This species was considered by our group as a role model for the study of regeneration due to several reasons: 1) high abundance in the Portuguese coast; 2) easy maintenance in a controlled environment; 3) high genome homology (70%) with humans [22]; 4) disposable of great quantities of CF to harvest and use for studies purposes at one single moment; 5) extraordinary regenerative capacity

to regenerate body parts or at most full individual regeneration followed by self-induced or traumatic amputation if only a fifth of the central disk remains attached to the lost arm [4, 23-24]; 6) the anatomical position of the nerve cords are “external” and easily accessible for experimental manipulation [23].

# 1.4. Biometrics

Animal biometrics is an approach to detect and represent, in a quantified way, the phenotypic appearance of individuals. Concretely can be used to measure morphological traits and their inter-individual variance [25]. Previous studies on the CF of *M. glacialis* regarding the protein characterization of the coelomic fluid free of cells (CFF) in the first phase of the regeneration process [26], and the characterization of circulating coelomocytes dynamics during regeneration [27], have found highly variable results due to biological variability. Since gender and the dimensions of an individual can play an important role in the biological variability of a given population, consequently, acting as factors of variability at a molecular level. Biometric measurement is a powerful technique that could diminish the inter-variability in regeneration studies. Many studies have used biometric measures as determinant parameters in asteroids. However, these studies are essentially intended to study predator-prey relationships, feeding, reproduction (spawning), and spatial density patterns. Biometric parameters used to characterize asteroids phenotypically are: 1) fresh weight [28-30]; 2) the total length of the animal or the maximum tip-to-tip diameter (arm-span), as the length of the tip of one arm to the opposite one [20-21, 30-32]; 3) length of the longest arm as the radius from the center of the disk to the tip of the longest arm [32-36]; 4) radius from the edge of the disk to the end of a normal arm on the opposite side [37]; 5) normal arm length [38-40]; 6) average linear distance from the tip of each arm to the opposite angular point [29,41]; 7) major radius [42]; 8) longest arm [28]; 9) arm width [30, 43]; 10) arm height [30, 43]; 11) arm length opposite to the madreporite [44].

# 1.5. Coelomic Fluid Cellular Populations

The coelomocytes, also designated as echinoderm blood cells, immune cells, or free rooming cells, are a set of cellular morphotypes present in the coelom. They are not only important for immunity but also play a key role in the regenerative process. Concretely, many cell types are mobilized to the site of injury to protect the inner environment that is susceptible to the foreign material, to heal the wound, and to restore the missing structures [2,15].

In *M. glacialis*, four types of coelomocytes were detected and distinguished through light microscopy: spherule cells, vibratile cells, amoebocytes, and phagocytes, the last ones being able to alternate between petaloid and filapodial morphologies [19]. More recently, Andrade and colleagues [45] resorting through flow cytometry (FC), went further and were able to characterize minutely two populations of coelomocytes, denominated as P1 and P2. Namely, the two different cell populations differed substantially in abundance, cell size, cell morphological complexity, and incorporation of fluorescence values. When analyzed ultrastructurally, the P1 population was constituted by two subpopulations of cells: 1) haploid cells, with low mitotic activity, undifferentiated cytotype and high nucleus/cytoplasm ratio, resembling stem-cells and proposed to be the progenitor cells of coelomocytes; 2) diploid cells, with the nucleus occupying most of the cell and thought to be a more differentiated state of the haploid cells (**Figure 1.5 A**). Regarding the P2 population, the ultrastructural analysis by flow cytometry imaging (IFC) revealed two main morphotypes similar to phagocytes, designated as petaloid

and filopodial cells, and to vertebrate thrombocytes, called regular (polygonal) and big granulated cells (**Figure 1.5 A**). Additionally, two other morphotypes were observed only by fluorescence microscopy (**Figure 1.5 B**) [45]. Functionally, thrombocytes, as the name implies, have a similar role to the human platelets when the starfish suffers an injury. These cells migrate to the site of lesion and form a clot that protects the inner from the outer environment, being, therefore, essential in the initial stage of the regenerative process triggered by a traumatic lesion [23]. The phagocytes also perform major roles in this initial phase, being fundamental in the phagocytic activity against pathogens, as well in contact with the lesion site the petaloid form undergo to the filopodial form, forming a network that allows the clot formation by the thrombocytes [23, 45].

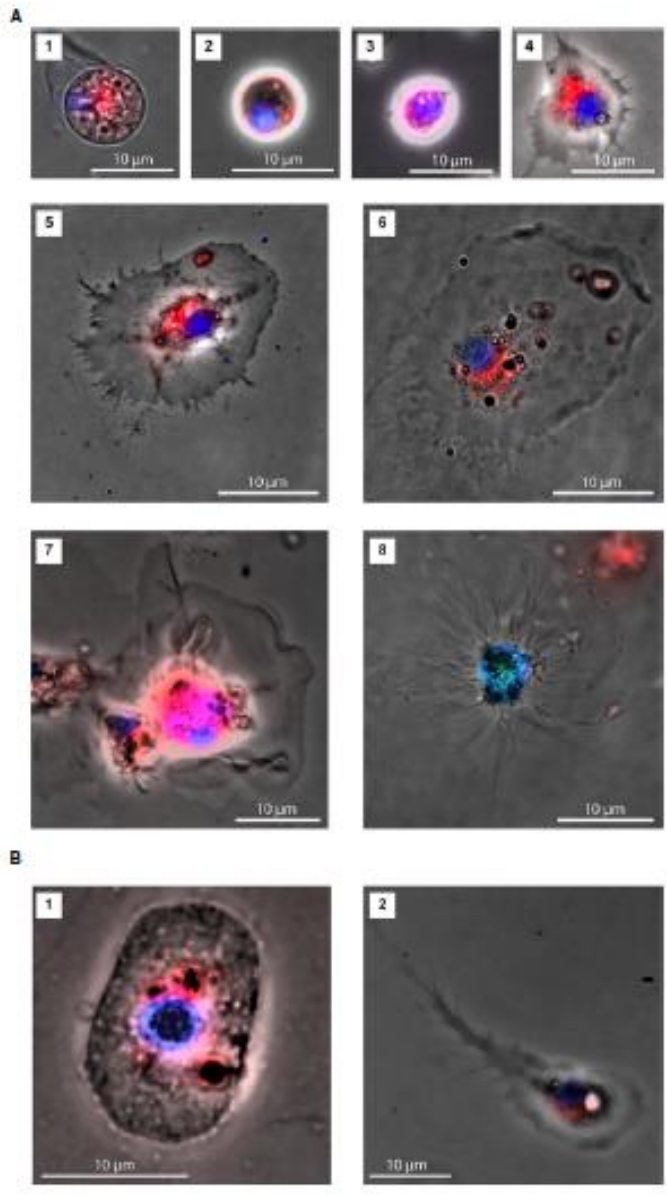


**Figure 1.5.** Coelomic fluid cell morphotypes detected in *M. glacialis* and characterized by fluorescence microscopy. (**A**) Two morphotypes were described in population P1, the small nucleus/cytoplasm ratio cell (**1** and **2**) and the high nucleus to cytoplasm ratio (**3** and **4**), as well in population P2, the thrombocytes (**5** and **6**) and the phagocytes (**7**- petaloid, **8**- filapodial). (**B**) Additionally, two novel morphologies that are only observed by fluorescence microscopy (**1** and **2**). Adapted from [45].

# 1.6. Regeneration

After all, what is Regeneration? Basically, it is a process that repairs and replace cells, tissues, organs, and body parts of a given organism, when subjected to amputation (through predation), self-induced autotomy (through predation defense or asexual reproduction), or traumatic lesion, rapidly followed by a complete successful re-growth of the lost parts [23,46]. Is an intrinsically conservative post-embryonic developmental process, starting from somatic cells and taking place in individuals at the adult or larval stages, that is crucial for individual survival and provides a necessary complement for the asexual reproduction program [23,47]. Ultimately, it is an extremely complex developmental process implying the coordination of different tissues, cells, and signals, requiring new cell recruitment and detailed spatial information to specify, both morphology and anatomically, the identity of the new tissue [23, 47-48].

This phenomenon is reached by different strategies, such as the rearrangement of pre-existing cells, the proliferation and differentiation of adult somatic stem cells, and the de-differentiation and/or trans-differentiation of cells. Specifically, de-differentiation is the process where a differentiated cell loses its tissue-specific characteristics becoming undifferentiated. Then these undifferentiated cells can re-differentiate into cells of their original tissue (re-differentiation) or to a cell of a different lineage (trans-differentiation) [49]. In echinoderms, regeneration implies the existence and availability of multipotent/pluripotent cells, that can be either undifferentiated pluripotent stem cells (adult stem cells) present in the circulating fluids or in the tissues in the form of resident cells [24], and/or cells derived from local existing tissues trough processes of de-differentiation [48]. The pyloric caeca and the coelomic epithelium have been proposed as sources of presumptive stem/progenitor cells, but in both cases, de-differentiation of the highly specialized cells of these tissues probably occurs before recruitment [47-48]. Meaning that there is a predomination of tissue-specific recycling of specialized cells generated from nearby tissues over the use of resident stem cells. In which these progenitor cells originate restricted types of cells, and cells of each tissue regenerate elements of the same tissue. However, there is an exception, of which the coelomic epithelia may generate the coelomocytes, cells of the muscle, and probably cells of the skeleton [48]. Related to the regeneration process, morphallaxis is the main process and probably the only one in asteroid regeneration. This process is characterized by the rearrangement/recycling that happens from only limited and localized proliferation activity involving cells derived from existing differentiated tissues by reversal of differentiation and/or migration [48]. Nonetheless, the other mechanism known is epimorphosis, often associated with regrowth of limbs of vertebrates, and that requires the formation of a blastema (a mass of undifferentiated cells) in the wound and consequent intensive cell proliferation to restore the lost body part [49-51]. According to the theory of the recruitment of resident stem cells, regeneration capability and potential can rely upon: 1) the individual potential for histogenetic and morphogenetic plasticity expressed in terms of recruitment of adult pluripotential cells (stem cells and/or dedifferentiated cells), followed by cell potential for proliferation and migration; 2) supply of specific regulatory/trophic factors; 3) and finally the expression, or re-expression, of a specific developmental program [24, 46].

Interestingly, recent studies underlined a certain homology between the chordates neural tube and echinoderms CNS and that the radial glial cells share significant morphological similarities with the radial glial of chordates, a cell type with high abundancy in embryogenesis of higher vertebrates [6]. Molecular studies also revealed that neuro-regeneration in Echinodermata also involves the extensive phosphorylation of proteins of the RNC [53], the presence of pluripotency factors orthologs with Yamanaka factors of the mammalian cells [54], the expression of Hox gene homologs [55], the action of growth factors, neuropeptides, and neurotransmitters [56], and related proteins with prolific roles [57]

in a similar fashion to what happens to vertebrates. For all the reasons above, echinoderms provide valuable models, closely related to vertebrates, for integrated studies related to reparative regeneration and stem-cell biology [52,58].

The molecular, cellular, and tissue mechanisms are well characterized in the regeneration triggered by autotomy or post-traumatic amputation of the arm in sea stars. However, the pathways of regeneration specifically only triggered in the RNC are still poorly characterized**.** Recently, in sea cucumbers, was made the first characterization of the nerve regeneration triggered by the amputation of a small section, based on morphological criteria. The regeneration consists in four phases: 1) *Early post-injury phase (1-2 days)*, where the glial cells of the ectoneural and hyponeural epithelia of the wound site experience differentiation, along a relative short distance of the plane of injury; 2) *Late post-injury phase (6-8 days)*, where the differentiation zone of the neuroepithelia spreads into deeper regions, and the differentiated glial cells seals the epineural and hyponeural canals in the wound area ; 3) *Growth phase (8 – 12 days)*, the CE seals the wound and the two regenerate portions of the RNC start growing towards each other across the wound gap beneath the CE, with the differentiated tips of the nerve forming thin tubular outgrowths, consisting of differentiated flat glial cells and very few neuronal elements, penetrating into the connective tissue that filled the gap; 4) *Late regenerate (21+ days post-injury)*, the two regenerate tips meet and fuse restoring the anatomical continuity of the nerve, with similar cellular structure and morphology of the non-regenerative part of the RNC, becoming equal with longer time [11]. A fundamental aspect is that the regeneration in starfishes is nerve-dependent, which is necessary for the individual to maintain a fully functional CNS in order to regrowth lost body parts. According to the literature the glial cells are involved in adult neurogenesis, as adult stem cells acting as the primary source of progenitor cells that forms new glial and neuron cells, or as niche cells, in which they control the mitotic activity, differentiation, and fate of the progenitor cells [9, 11].

# 1.8. Thesis Aims

The main goal of this study was to answer the question: what does the post-traumatic regeneration of the RNC trigger in terms of molecular, cellular, and tissues levels? To achieve this goal, a small section of the nerve was amputated and the dynamics of the IS, specifically the proteins quantity, and the changes in the coelomocyte's populations, as well the tissues patterns of the arm section around the nerve, were characterized at three different regeneration times (1, 7 and 14 days post-traumatic amputation). The CFF proteins were quantified by BCA assay, with the additional objective to be characterized and identified through liquid chromatography with tandem mass spectrometry (LCMS-MS). The coelomic fluid cellular populations were studied through FC, in terms of abundancy, optical characteristics, and morphology. Moreover, the arm tissues profile and the involvement of the neighboring tissues were characterized to understand the histological and morphological patterns of the regenerating nervous tissue, through microscopy anatomy resorting to histology tools.

This study had other objectives not less important, such as: 1) to describe the population of asteroids in terms of dimensions and relations among their sizes and weight, and consequently to find biometric measures that can distinguish and predict the sex of the specimens; 2) to compare the quantification of proteins in the CFF between gender; 3) to further characterize morphologically and define differentiation characteristics between the subpopulations of coelomocytes, previously described [45];

# 2. MATERIALS AND METHODS

In **Figure 2.1** is presented a summary of the experimental workflow in accordance with the objectives of this study, which will be explained in more detail in the following sub-chapters.

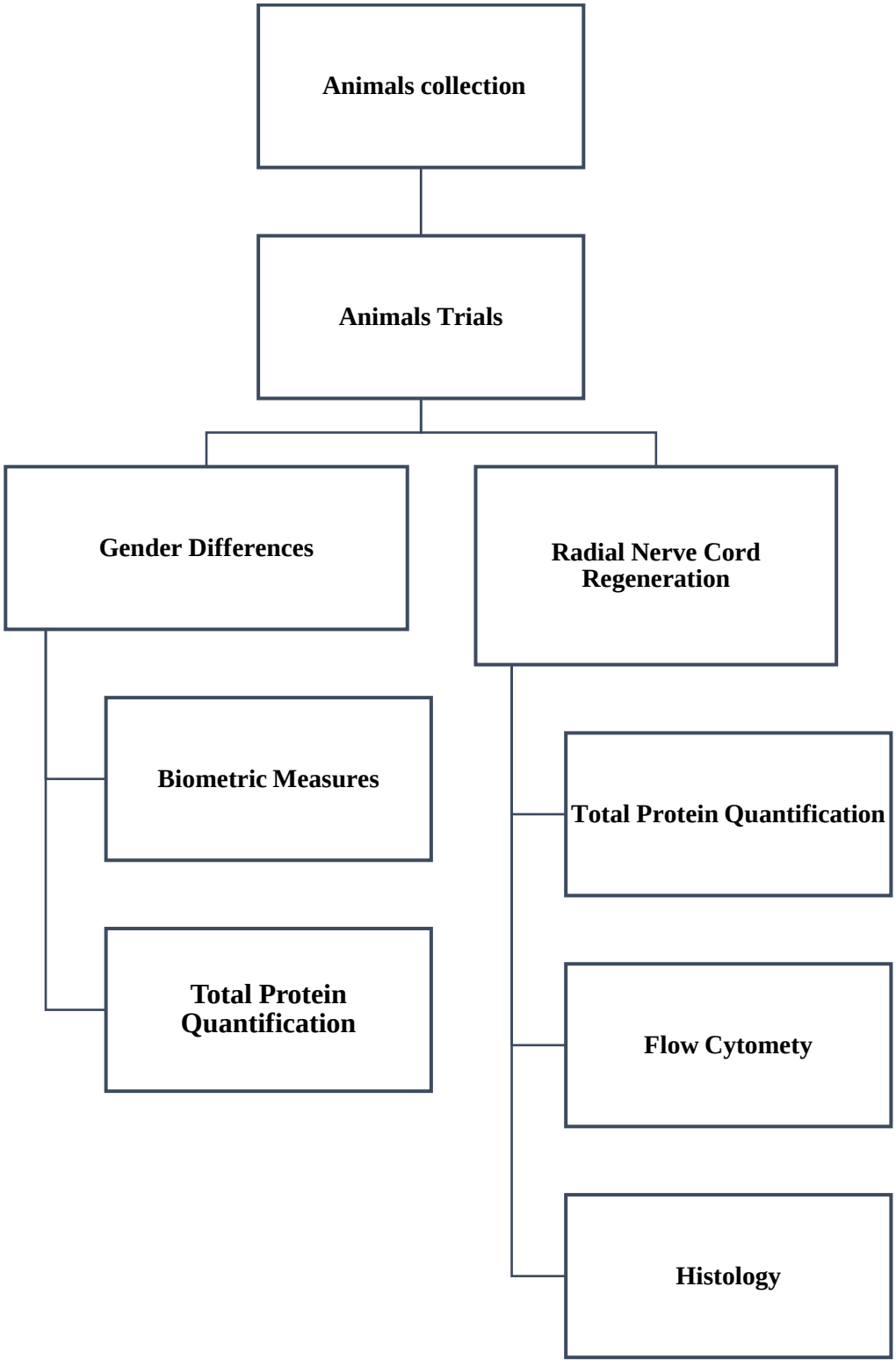


**Figure 2.1.** Scheme of the study objectives according to experimental methodologies.

# 2.1. Animals Trials

## Animals Collection

Specimens of *M. glacialis* were collected in the intertidal zone on the east coast of Portugal, in Praia da Poça (São João do Estoril) (38.702052º N, 9.392640º W) (**Figure 2.1.1**).


**Figure 2.1.1.** Location of the sea star´s collection site (São João do Estoril, Praia da Poça).

The collection occurred outside the breeding season in two batches, previously in February 2019 and in January 2020, during the morning period at low tide. Were collected firstly 45 and secondly 65 adults without recent signals of arms regeneration or injury or pigmentation defects in the epidermis. Collected animals were placed in captivity at Aquário Vasco da Gama (Oeiras, Dafundo) in open circuit tanks with recirculating water, with a temperature of 15ºC and salinity of 33‰, fed ad libitium on a mussel's diet (**Figure 2.1.2**).

**Figure 2.1.2.** *M. glacialis* populations at Aquário Vasco da Gama (Dafundo, Oeiras).

Starfish were therefore kept in the same conditions throughout the project, to avoid variability caused by abiotic factors, such as temperature and salinity. Prior to the experimental procedures, starfish were subjected to an acclimation period of 15 days, in order to monitor the animal´s tenacity and weakening of the thorns. Animals showing this behavior were discarded.

# Biometrics

Biometric measures were performed by a photographic method using the aboral view of the asteroids (see Attachment 1). Alongside a ruler was used as a scale and each image was processed with the ImageJ software (https://imagej.nih.gov/ij/). In the software, 1 cm was measured from the ruler to transform the scale of pixels to centimeters, and measurements were determined by segmented line to the nearest 0,1 mm.

From the first date of collection, 45 individuals, and from the second date, 23 individuals, were weighed and later measured on the aboral side. The determined parameters were the length of each arm to the center of the central disk (Al), the width of each arm (Aw), and the diameter of the central disk (CDd), as depicted in **Figure 2.1.3**. Al was measured from the tip of each arm to the anus (the medial point of the central disk). Aw was determined from the middle point between the two first thorns on one lateral row to the middle point between the two first thorns of the opposite lateral row. The CDd (see **Figure 2.1.3**) was calculated by the average of the distance (here referred as the diameter of a given arm) between the first thorn of the middle row in each arm to the extremity of the central disk between the two arms opposite to the initial one. The weight (W) was determined as soon as the animals were taken from the water with the aid of a technical balance.

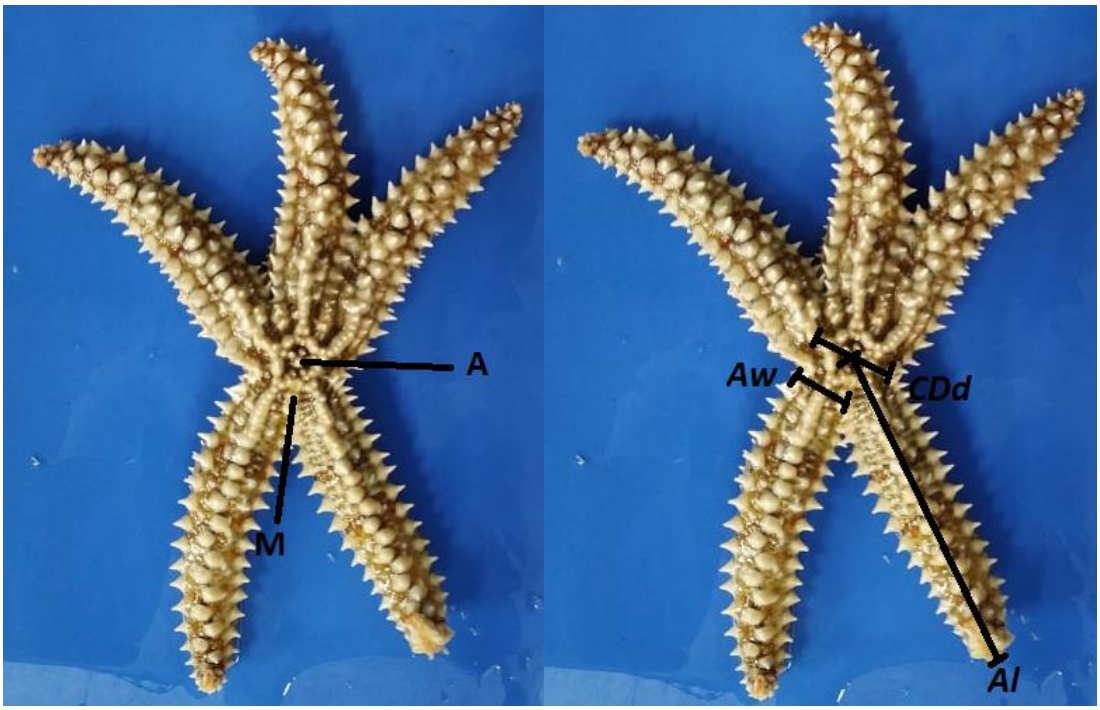


**Figure 2.1.3**. Aboral view of a *M. glacialis* specimen showing, on the left side the identification of the anus (A) and the madreporite (M); and on the right side the biometric parameters measured: arm width (Aw), arm length (Al) and central disk diameter (CDd).

Through the described measurements were calculated for each animal the mean arm´s length (*xAl*), mean arm´s width (xAw) and, consequently, the ratios between mean arm´s width and mean arm´s length (xAw/xAl), central disk diameter and mean arm´s length (CDd/xAl), mean arm´s width and central disk diameter (xAw/CDd), mean arm´s length and weight (xAl/W), mean arm´s width and weight (xAw/W), central disk diameter and weight (CDd/W), finalizing the constitution of the group of biometric parameters used in this study.

## Sex determination

Starfish gender was determined by visual inspection of the gonads. It was done concomitantly with the collection of the samples for histological analysis. This allowed disturbing the individual only once without compromising the experimental results. Specimens were classified as males if their gonads appear to have a yellowish/white color, or as females, if their gonads appear to have an orange/reddish color (similar as in [37]).

## Induction of regeneration

The induction of the regeneration process and the collection of tissues was carried out in arm number 1 (first arm immediately to the right of the madreporite). Prior to regenerative induction, the sea stars were anesthetized with 4% (w/v) of magnesium chloride in seawater. After the individuals were

relaxed, induction of nerve regeneration was triggered by cutting with a scalpel a small section (around 1 cm) of the radial nerve close to the tip of the arm (at around 1 cm from the arm tip) (**Figure 2.1.4**).

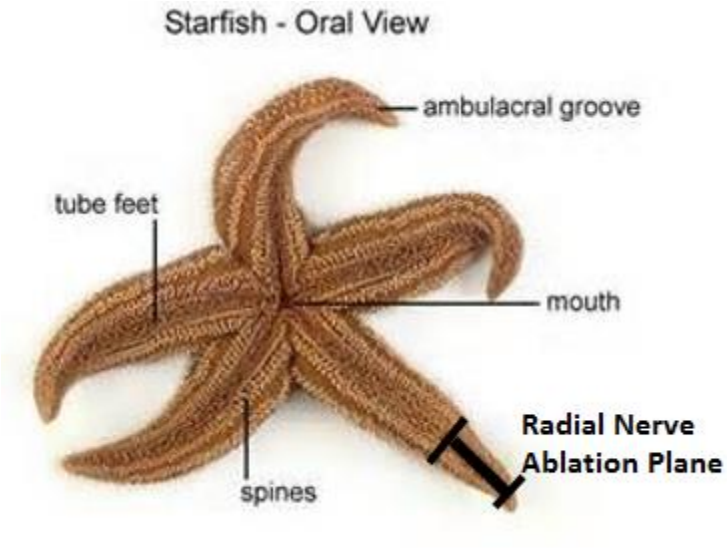


**Figure 2.1.4.** Representation of the ablation plane of the RNC.

# Coelomic fluid harvest

CF was harvested aiming at total protein quantification and flow cytometry characterization of coelomocyte populations. The epidermis at the arm tip was perforated with a 21-gauge-butterfly needle. By gravity, the fluid was collected into a falcon tube, stored in ice, and carried out to the laboratory (**Figure 2.1.5**).

**Figure 2.1.5.** Collection of the coelomic fluid.

## Arm tip collection

The collection of the arm section for histological analysis occurred through the horizontal incision, approximately two-thirds to the base of the arm, above the incision plane of the radial nerve. The tissues were then preserved on an ice bath in a falcon tube in the Bouin fixative (71,42 mL of a saturated solution of picric acid; 4,76 mL of glacial acetic acid 100%, and 23,80 mL of formaldehyde 37%). Then were carried out to the laboratory and stored at 4º C.

# 2.2. Radial Nerve Cord Regeneration

The study of the dynamics of the initial phase of the RNC regenerative process was carried out in a phased manner for each of the experimental procedures, over three-time points (1 day, 7 days, and 14 days). At each time point after the induction of the RNC regeneration, CF was harvested for protein´s quantification analysis and flow cytometry analysis, and the arms of each specimen were collected for histological analysis (**Figure 2.2**). For the dynamics of the circulating proteins the control group, in which regeneration was not induced accounted 10 biological replicas, the time point 1 day accounted for 6, the time point 7 days only accounted for 4, and the timepoint 14 days accounted for 5 replicas. For the CF analysis, the control group accounted 2 replicas for each time point, and each time accounted for 5 replicas. For the histological analysis, each regeneration experimental group consisted of 5 individuals, and each control group consisted of 3 individuals.

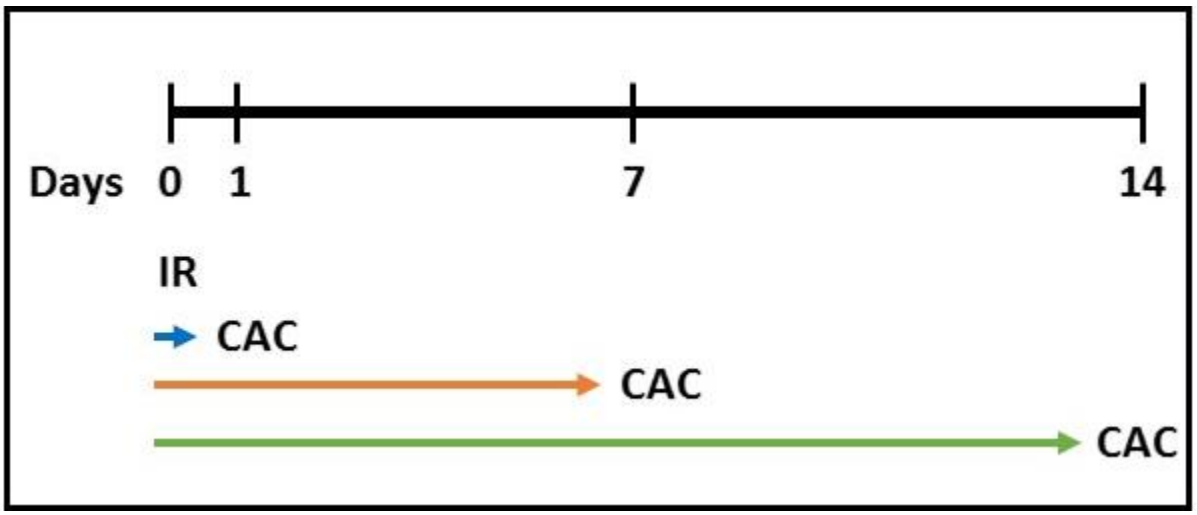


**Figure 2.2.** Workflow of the post-traumatic regeneration experimental procedure in days, 1, 7 and 14. **IR**- induction of the regenerative process; **CAC**- coelomic fluid and arm collection of each experimental group.

# 2.3. Cell-free coelomic fluid total Protein Quantification

After harvesting, the CF was separated into two fractions by centrifugation for 5 min at 1,000 x *g* and at a temperature of 4 ºC. The pellet contained the circulating cells (coelomocytes) was discarded, and the supernatant consisted of the cell-free coelomic fluid (CFF), which contained the solubilized proteins.

In order to obtain a protein concentrate, samples of the CFF were precipitated in a 1:1 (v/v) proportion with 40% trichloroacetic acid (TCA), in the presence of 0.028% β-mercaptoethanol, and

subsequently, incubated overnight at 4ºC. To obtain a protein pellet, the suspensions obtained were centrifuged for 30 min, at a speed of 10,000 x g and at a temperature of 4ºC. To remove residual TCA, the pellet was washed three times with acetone in an ice bath between centrifugations (carried out under the same conditions as those previously described) and dried at room temperature, overnight. Then, the pellet was dissolved in a solution of 6 M of urea 50 mM of ammonium bicarbonate (AB). The protein concentration was determined with the Bio-Rad Protein Assay kit, based on the bicinchoninic acid (BCA) assay [59]. Therefore, 10 µL of each protein extract was placed in tubes with 40 µL of Dye Reagent Concentrate and 150 µL of bi-distilled water, making a final volume of 200 µL. The protein concentration was estimated based on the standard curve, performed through 6 dilutions of the standard protein solution (1.0 mg/ml of bovine serum albumin in 0.15M NaCl with 0.05% sodium azide), according to **Table 2.3**.

**Table 2.3.** Volume of the 6 dilutions of the BCA calibration curve.

| **Standard Protein Concentration (µg/mL)** | **Volume (µL)** | | | | |
|---|---|---|---|---|---|
| | **Standard Protein** | **$H_2O$** | **Buffer Solution*** | **Dye Reagent Concentrate** | **Final Volume** |
| 0 | 0.0 | 150.0 | 10 | 40 | 200 |
| 8 | 1.3 | 148.7 | | | |
| 15 | 2.4 | 147.6 | | | |
| 30 | 4.8 | 145.2 | | | |
| 50 | 8 | 142.0 | | | |
| 80 | 12.8 | 137.2 | | | |

Note: * 6 M Ureia 50 mM AB solution.

Solutions were incubated for 30 min at room temperature, and 200 µL of each sample and each standard protein solution were placed on a 96-well ELISA plate. Absorbances were measured at a wavelength of 595 nm by the plate reader Epoch (Biotek), resorting to Gen5 software (Biotek). The absorbance values of the dilutions allowed to obtain a standard curve. Protein concentration in the CFF protein extracts were calculated using the standard curve equation and the absorbance values of the samples. Consequently, the protein quantity was assessed for the total CFF volume, which was measured posteriorly to the CF separation and previously to the protein precipitation (see Attachment 2).

# 2.4. Characterization of coelomocyte populations by Flow Cytometry

## Traditional flow cytometry (FC)

Coelomocytes populations at three regeneration time-points were characterized through FC. This allowed the detection, differentiation, and characterization of coelomocytes populations based on their cellular characteristics, such as size, shape and roughness, and incorporation of DRAQ5/fluorescence values. The number of cells in % of each population was also determined. After the collection process of the CF, the samples were transported in an ice bath, of the Aquário Vasco da Gama to the laboratory. In order to minimize the aggregation of cells, and no changes in their conformation would occur that would interfere with the readings, all samples had to be resuspended by means of a micropipette. Prior to the FC methodology, the samples were processed by filtration through a 30 µm mesh, to prevent capillary coagulation. First, the samples were stained with DRAQ5 (Thermo Fisher Scientific, # 65-0880-92; DNA). Then, the samples were analyzed in a CyAn ADPTM flow cytometer (Beckman Coulter), incorporated with the Summit ™ software, and separated according to the cell type using the High-Speed Cell Sorter flow cytometer, LSR Fortessa ™ (BD Biosciences). For the optimal optical configuration for each flow cytometer, 665/20 BP and 660/20 BP (LSRFortessa ™) filters, and 642 and 633 nm lasers were used, respectively for Cyan ADPTM and LSRFortessa ™ cytometers. The data obtained by the FC was subsequently analyzed using the software FlowJo (version 10.7, Becton, Dickinson & Company). To obtain the relation of the morphologic and fluorescence characteristics of the cells, a specific gating strategy was implemented. First, the relation between APC-Cy 7 (tandem fluorochrome) and DRAQ5 intensity allowed to obtain the living cells. Then, the relation between SSC-A (area) and SSC-H (height) was used to select the single cells and remove the aggregates. The characterization of the cellular populations was made based on the DRAQ5 intensity and SSC-A values.

## Imaging flow cytometry (IFC)

Flow cytometry coupled to an imaging system using the INSPIRE software of the ImageStreamX Mark II imaging flow cytometer (Luminex Corporation, Austin, TX) was used to acquire images of coelomocytes *via M. glacialis* individuals in a non-regenerative state, obtained in Andrade *et al*., (2021) [45]. Using these images, this study intended to associate specific morphologic characteristics for the characterization of each subpopulation, resorting to the software IDEAS (version 6.2). The analysis was made using the tool "Feature Finder Wizard", which is a process that sets morphological features that separate two different phenotypes (IDEAS User Manual 6.0). The gating strategy passed through the selection of the focused cells analyzing the relation between normalized frequency and root mean square (RMS) gradient. Then, single cells were obtained through the relation between aspect ratio and the area of the cells, features of the bright field channel. Next, the cells were selected visualizing the bright field images, and attributed to the subpopulations of populations 1 and 2. Then, were selected the channels of the bright field image (1 and 9), side scatter (SSD) (1), FM 4-64 marker intensity (5), and DAPI intensity (channel 7) and their corresponding morphological and optical characteristics to obtain the best features of discrimination. The morphologic characterization was made based on the mean of the risk difference (RD mean) and the plots of the two best discriminator characteristics.

# 2.5. RNC Regeneration Patterns through Histology

Histology was accessed through light microscopy for morphological characterization of the RNC p.a. regeneration to understand the involvement of the RNC and surrounding tissues in this process. Collected arm tips (chapter **2.1. Animals Trials**) from regenerative and non-regenerative animals were maintained for 2-3 months at 4º C in Bouin solution with 3x the volume of the sample. The Bouin solution was changed once a week in the first month, and once a month in the following ones. Then, samples were processed by several washing steps, with the help of an orbital shaker, previously being placed in the mold of paraffin (**Figure 2.5**).

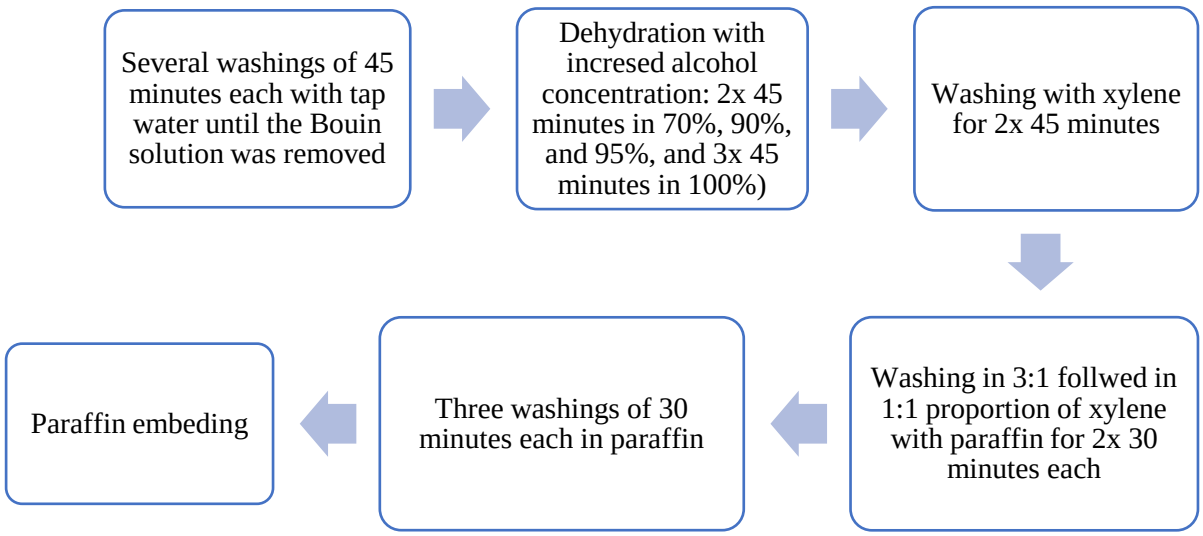


**Figure 2.5.** Workflow of the washings to remove the Bouin solution and prepare the samples for paraffin embedding.

Paraffin embedded samples were orientated according to the sagittal plane of sectioning and left overnight at room temperature. The sectioning of the samples was performed with a Leitz 1512 rotary microtome, with a thickness of about 7-10 µm conforming with the size of each sample. 2 or 3 sample slices were placed on top of a glass slide. Those serving the purpose of this study, showing the nerve gap or the total nerve tissue, were stained following Milligan's Trichrome procedure [60] (**Table 2.5**):

**Table 2.5**. Milligan's Trichrome staining procedure.

| Step | Task | Time (min) |
|---|---|---|
| 1 | Washing in xylene | 20 |
| 2 | Re-hydration in ethanol 100% | 4 |
| 3 | Re-hydration in ethanol 95% | 2 |
| 4 | Slides placed in AB solution (potassium dichromate 3% + hydrochloric acid in ethanol 95%) | 5 |
| 5 | Washing in distilled water | |
| 6 | Staining with acid fuchsin 0.1% | 4 |
| 7 | Washing in distilled water | |
| 8 | Fixation in phosphomolybdic acid 1% | 3 |
| 9 | Staining with Orange G | 4 |
| 9 | Washing in distilled water | |
| 10 | Slides rinsed in acetic acid 1% | 2 |
| 11 | Staining with Fast Green | 3 |
| 12 | Slides in acetic acid 1% | 3 |

After staining, the tissue slices were dehydrated with ethanol 95% for 2 minutes and with ethanol 100% for 4 minutes, then washed in xylene for 2 minutes and transferred to clean xylene until the slides were mounted with Eukitt® (5% acrylic resin and 55% xylene mounting medium). Slides stayed overnight at room temperature until Eukitt® was completely dried. Then, the stained sections were observed under a Leitz Wetzlar light microscope and photographed with a Leica EC3 Camera and Leica Application Suite LAS EZ Software (Version 1.8.0).

# 2.6. Statistical Analysis

To differentiate the gender based on biometric parameters (chapter **2.1. Animals Trials**) and evaluate gender influence in the total CFF protein quantification. Exploratory methods of the data, correlation analysis, two-sample tests, and variance analysis were accessed using RStudio (version 4.0.3) software, and principal component analysis (PCA), discriminant analysis (DA), specifically partial least square discriminant analysis (PLS-DA), and predictive power analysis, were accessed using the platform MetaboAnalyst (version 5.0). Shapiro-Wilk and Bartlett tests were performed on the entire sample data, to ensure compliance with the assumptions of normality of distribution and normality of variance, respectively, for further statistical analysis. The coefficient of variation was calculated for the means of each variable to evaluate biological variability. Correlation analysis between each biometric

parameter, and with the total CFF protein quantification was performed using correlation coefficients of Pearson (r), or Spearman (p) when data normality was not observed. Two-sample tests (t-test or Mann-Whitney) were also used to evaluate the existence of biometric parameters and CFF total protein with significant differences between gender. Finally, for further analysis, two multivariate analyses were performed. Previously, the data was normalized through autoscaling so that each parameter had the same statistical relevance. Then, on one hand, principal component analysis (PCA) was assessed the discrimination between gender by the measured variables. On the other hand, PLS-DA was evaluated consonant the gender to obtain prediction functions for future specimen's sex determination. Statistical analysis was assessed considering a confidence level of 0,05.

In respect of the RNC regeneration process, the dynamics of the circulating proteins in the CFF and cellular populations in the CF, data obtained by the BCA quantification, and the % of cells acquired through FC respectively, were evaluated through a two-sample test. Statistical difference was accessed between each regeneration time-point, and them with the control group, following the same rules explained above. Also, the two-sample test was performed for the CFF total protein quantification determined through the CF collection on two different days, in the same individuals used for the regenerative experiments, but in a non-regenerative state.

# 3. RESULTS AND DISCUSSION

## 3.1. Sex Differentiation

Asteroids are one of the most diverse groups within the phylum Echinodermata, that occurs at all depths from the intertidal to the abyssal in every ocean of the globe, that occupy different types of niches and types of ecological roles [61]. It is well known that inter-individual diversity is one of the most important factors in ecological and evolution success through the times and since the beginning of life [62]. Variance in M. *glacialis* populations is no exception, displaying varied forms of population dynamics, habitats occupied, reproduction, several pray of choice, different body colors, body sizes, among others [4,20].

### Biometrics shows another evidence that *M. glacialis* do not display sexual dimorphism

A population with high variance in genotype and phenotype is less susceptible to environmental changes determining a high ecological success [62]. In this study, phenotypical differences between gender and starfish, in general, were assessed through biometric parameters (see Attachment 3). The most usual biometric measure used to describe morphologically the *M. glacialis* is the total body length. However, its values are not consensual. For example, Bay-Nouailhat (2005) [63] describes the adults of *M. glacialis* to have on average between 30 to 40 cm in diameter and can reach 80 cm. However, Ager (2008) [64] describe this species to have a common size between 25 to 30 cm and can grow to 70 cm. The specimens from the present study exhibits this phenotypical variance in terms of body sizes from an intertidal population of *M. glacialis*. Even though coefficients of variance were relatively low, none of them were lower than 10%. Subsequently, in just 68 individuals, could be witnessed in a statistical level, a wide interval of W, Al, Aw and CDd (**Table 3.1.1**).

**Table 3.1.1.** *M. glacialis* determined biometric measures, **W**- all body wet weight; **xAl**- mean arm´ length; **xAw**- mean arm´s width; **CDd**- central disk diameter. Range (**minimum** and **maximum**), **mean ± s.d** (standard deviation), and coefficient of variation (**CV**) of biometric measures. N=68.

| | **W(g)** | **xAl (cm)** | **xAw (cm)** | **CDd (cm)** |
|---|---|---|---|---|
| **Minimum** | 53,56 | 7,24 | 1,29 | 1,38 |
| **Maximum** | 342,84 | 15,67 | 3,150 | 3,42 |
| **Mean ± s.d** | 122,52±57,33 | 10,37±1,70 | 2,05±0,35 | 2,25±0,56 |
| **CV (%)** | 47% | 16% | 17% | 25% |

As a matter of fact, the size of asteroids plays a major role in their predatory activity, and consequently, in diet composition and foraging behavior. Small starfish tend to consume algae, epifaunal turfs, and small gastropods contrasting with bivalves and carrion consumed by larger individuals [35]. Specifically, *M. glacialis* tend to select mussels by their sizes as a mechanism to maximize net energy

gain, in which the size and number of mussels consumed increase with sea stars Al [34]. Previous studies in other asteroids species showed that increased food supply potentially increases growth, gonad development, and pyloric caeca index, which consequently increases energy storage, an important factor in the regulation of arm regeneration [65-66]. Moreover, the length of the autotomized arm can be a relevant factor in the regeneration rate, since regeneration time is the same for any sea star, the bigger ones seem to have higher energy allocation to the regeneration than the smaller individuals [66]. Therefore, this issue can potentially be a determinant factor for different results in arm regeneration experiments, when attending to different size classes. Some starfish have different lengths and widths among their several arms, which at the outset the mean of these measurements are not good measures, since they ignore this morphological anomaly. However, despite the asymmetry of the arms, overall sea stars showed no significant differences and similar values in length (**A**) and width (**B**) of all arms (**Figure 3.1.1**). Thus, in this study, the average can be considered a good biometric measure to represent the length and width of all sea stars´ arms, mitigating measurement errors.

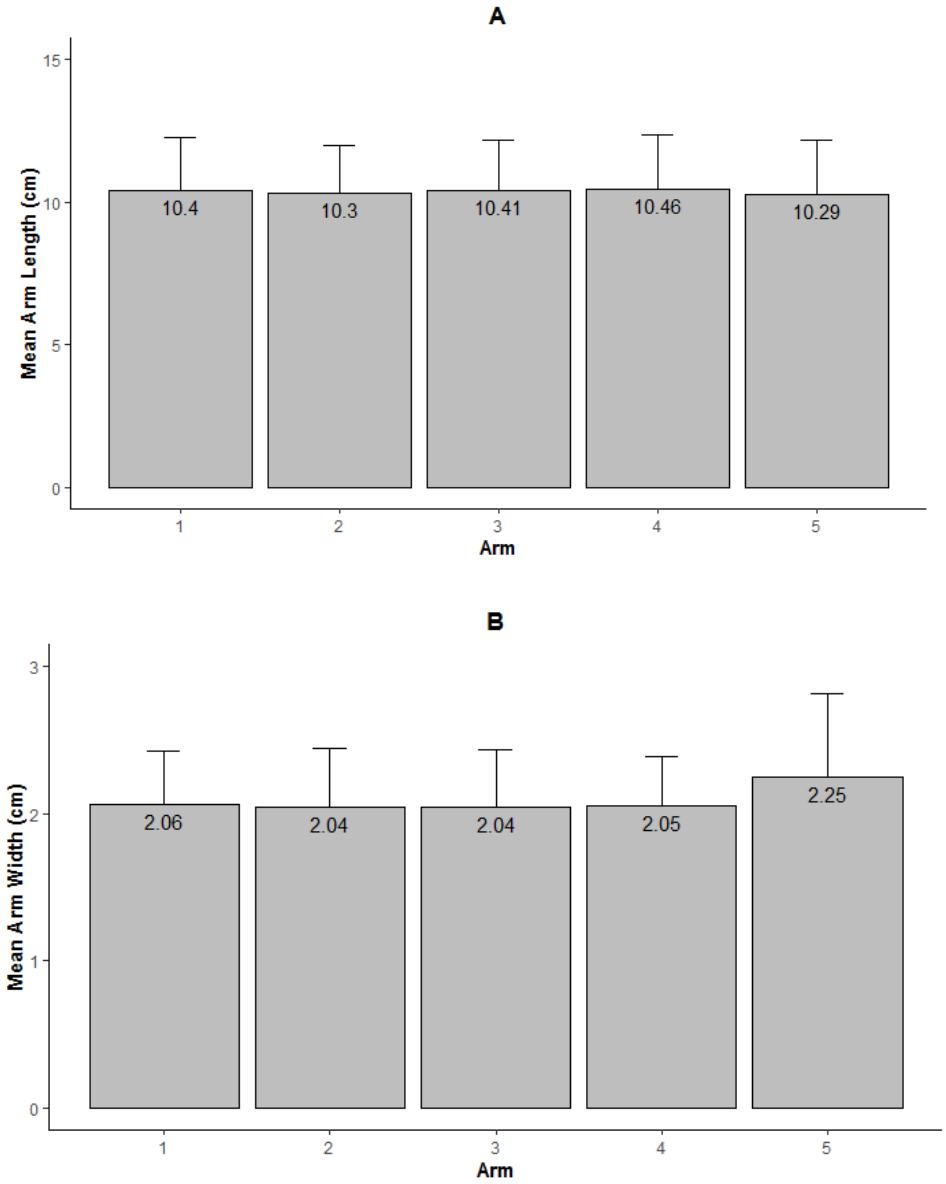


**Figure 3.1.1**. Mean length (**A**) and width (**B**) of each arm of 68 *M. glacialis* specimens.

Moreover, sea stars were evaluated for their phenotypic differences through the proportions between each measured body part length, and between them and weight (xAw/xAl, xAl/W, xAw/W, CDd/xAl, xAw/CDd, and CDd/W). As a consequence of the difference registered in previous measurements, sea stars also have wide ranges in terms of proportions (**Table 3.1.2**). In addition, stands out the evidence that Aw is about 20% of the Al and that the weight is represented by 10% of one Al (50% in total), 2% of one Aw (10% in total), and another 3% of CDd.

**Table 3.1.2.** *M. glacialis* determined proportions of the biometric measures, **xAw/xAl-** proportion between the mean arm´s width and the mean arm´s length; **xAl/W-** proportion between the mean arm´s length and the weight; **xAw/W-** proportion between the mean arm´s width and the weight; **CDd/xAl-** proportion between the central disk diameter and the mean arm´s length; **xAw/CDd-** proportion between the mean arm´s width and the central disk diameter; **CDd/W-** proportion between the central disk diameter. Range (**minimum** and **maximum**), **mean ± s.d** (standard deviation), and coefficient of variation (**CV**) of biometric parameters. N=68.

| | **xAw/xAl** | **xAl/W (cm/g)** | **xAw/W (cm/g)** | **CDd/xAl** | **xAw/CDd** | **CDd/W (cm/g)** |
|---|---|---|---|---|---|---|
| **Minimum** | 0,14 | 0,04 | 0,01 | 0,21 | 0,54 | 0,01 |
| **Maximum** | 0,27 | 0,16 | 0,03 | 0,35 | 1,02 | 0,05 |
| **Mean ±s.d** | 0,20±0,03 | 0,10±0,03 | 0,02±0,01 | 0,27±0,03 | 0,75±0,1 | 0,03±0,01 |
| **CV (%)** | 13% | 30% | 33% | 13% | 14% | 36% |

An important aspect to study biomass in invertebrates is the correlation between biometric parameters, such as weight and length [30]. To verify if there is an association between biometric parameters measured, correlation analysis was assessed, and was demonstrated that weight has a strong association with CDd, xAw, and xAl (**Table 3.1.3**). Previous studies have already demonstrated a positive correlation between weight and arm height (distance between the aboral to the oral extremities) and total length [30]. Consequently, arms height and the total length measures constitute reliable weight estimations [43]. Also, arm height is strongly correlated with total length, CDd, Aw and length of the longest arm [30]. Which, as expected in this study was found a correlation between xAl and xAw. However, the association between Aw and the total length was not found in the other study [43], which can be explained by the different measurement methods. Another interesting result in this study is the significant association between the CDd and the xAl and xAw, but with lesser strength for the first one than the other significant associations (**Table 3.1.3**). Existing correlation between the biometric measures as consequence, results showed that proportions between biometric parameters have a relatively lower coefficient of variance, i.e., less variation than the absolute measures, and therefore were also used to access morphological sexual differences.

**Table 3.1.3-** Pearson coefficient (r) or Spearman coefficient (p) and P-value) of the correlation test between biometric measures, **W**- weight; **CDd**- central disk diameter; **xAl**- mean arm´s length; **xAw**- mean arm´s width expressed in cm; and their proportions. N=68.

| **Biometric Parameters** | **Coefficient of Correlation** | **P-value** |
|---|---|---|
| *W* and *CDd* | p= 0.85 | <0.001 |
| *W* and *xAl* | p= 0.72 | <0.001 |
| *W* and *xAw* | p= 0.88 | <0.001 |
| *CDd* and *xAl* | p= 0.63 | 0.002 |
| *CDd* and *xAw* | p= 0.84 | <0.001 |
| *xAl* and *xAw* | r= 0.71 | <0.001 |

Settled the phenotypic differences between populations, it is also important to determine differences in genotype, since these two variables are inseparable when it comes to inter-individual variation [62]. However, it is difficult, costly, and time-consuming to assess genotypic differences. Since gender contributes to differences in genome level among individuals, a possible method to evaluate genotypic variability could be the gender differentiation *in situ* through biometrics. In this sense, the sex of 68 *M. glacialis* sea stars was determined, resulting in a total of 23 females and 26 males. For 19 individuals the sex was not possible to be determined due to the absence of the gonads, in consequence of a contracted disease, and due to sampling occurring outside the breeding season. In these situations, sex was classified as undefined. Thereafter, the differences between gender in terms of biometric parameters measured previously was evaluated for 49 individuals (**Table 3.1.4**). In this study, it was not found significant differences between genders. Even though some asteroid species have already been reported of having sexual dimorphism in size and in coloration of the body [67], sexual dimorphism is rare in echinoderms, and is not demonstrated and recognized in *M. glacialis* species.

**Table 3.1.4.** P-value of the t-test or Mann-Whitney test between genders, and their respective **means ± s.d** (standard deviation), evaluated in 23 females and 26 males, according to the biometric parameters, **Al1**- length of arm 1; **Al2**- length of arm 2; **Al3**- length of arm 3; **Al4**- length of arm 4; **Al5**- length of arm 5; **Aw1**- width of arm 1; **Aw2**- width of arm 2; **Aw3**- width of arm 3; **Aw4**- width of arm 4; **Aw5**- width of arm 5; **CDd**- central disk diameter; **xAl**- mean arm´s length; **xAw** mean arm´s width; **W**- weight; and the proportions of **xAw/xAl**, **xAl/W**, **xAw/W**, **CDd/xAl**, **xAw/CDd** and **CDd/W**.

| | **Females (mean±s.d)** | **Males (mean±s.d)** | **P-value** |
|---|---|---|---|
| **W (g)** | 144,53±65,84 | 125,43±57,58 | 0,220 |
| **Al1 (cm)** | 10,72±1,77 | 10,51±1,99 | 0,694 |
| **Al2 (cm)** | 10,80±1,63 | 10,26±1,71 | 0,136 |
| **Al3 (cm)** | 10,86±1,52 | 10,60±1,91 | 0,594 |
| **Al4 (cm)** | 10,73±1,70 | 10,63±2,09 | 0,602 |
| **Al5 (cm)** | 10,73±1,54 | 10,26±2,52 | 0,203 |
| **xAl (cm)** | 10,77±1,55 | 10,44±1,87 | 0,378 |
| **Aw1 (cm)** | 2,59±0,28 | 2,50±0,44 | 0,379 |
| **Aw2 (cm)** | 2,16±0,34 | 2,09±0,40 | 0,279 |
| **Aw3 (cm)** | 2,15±0,31 | 2,09±0,46 | 0,189 |
| **Aw4 (cm)** | 2,15±0,36 | 2,08±0,44 | 0,307 |
| **Aw5 (cm)** | 2,12±0,33 | 2,08±0,37 | 0,561 |
| **xAw (cm)** | 2,16±0,31 | 2,09±0,40 | 0,271 |
| **CDd (cm)** | 2,39±0,56 | 2,40±0,63 | 0,992 |
| **xAw/xAl** | 0,20±0,02 | 0,20±0,02 | 0,911 |
| **xAl/W (cm/g)** | 0,08±0,03 | 0,09±0,03 | 0,190 |
| **CDd/xAl** | 0,26±0,03 | 0,27±0,03 | 0,280 |
| **xAw/W (cm/g)** | 0,02±0,01 | 0,02±0,01 | 0,317 |
| **xAw/CDd** | 0,78±0,10 | 0,75±0,11 | 0,377 |
| **CDd/W (cm/g)** | 0,02±0,01 | 0,03±0,01 | 0,285 |

According to these results, also with the multivariance analysis was not possible to discriminate gender and to obtain a model predictive of males and females based on biometric parameters (**Figure 3.1.2 A** and **B**) and that this could not be achieved with a higher sample size (**Figure 3.1.2 C**). Meaning that the estimation of statistical power suggests that statistical model quality is not dependent on an increase in the number of individuals to be tested. Concluding that with these biometric parameters is not possible to distinguish males from females, becoming more evident that this species does not appear to display sexual dimorphism.

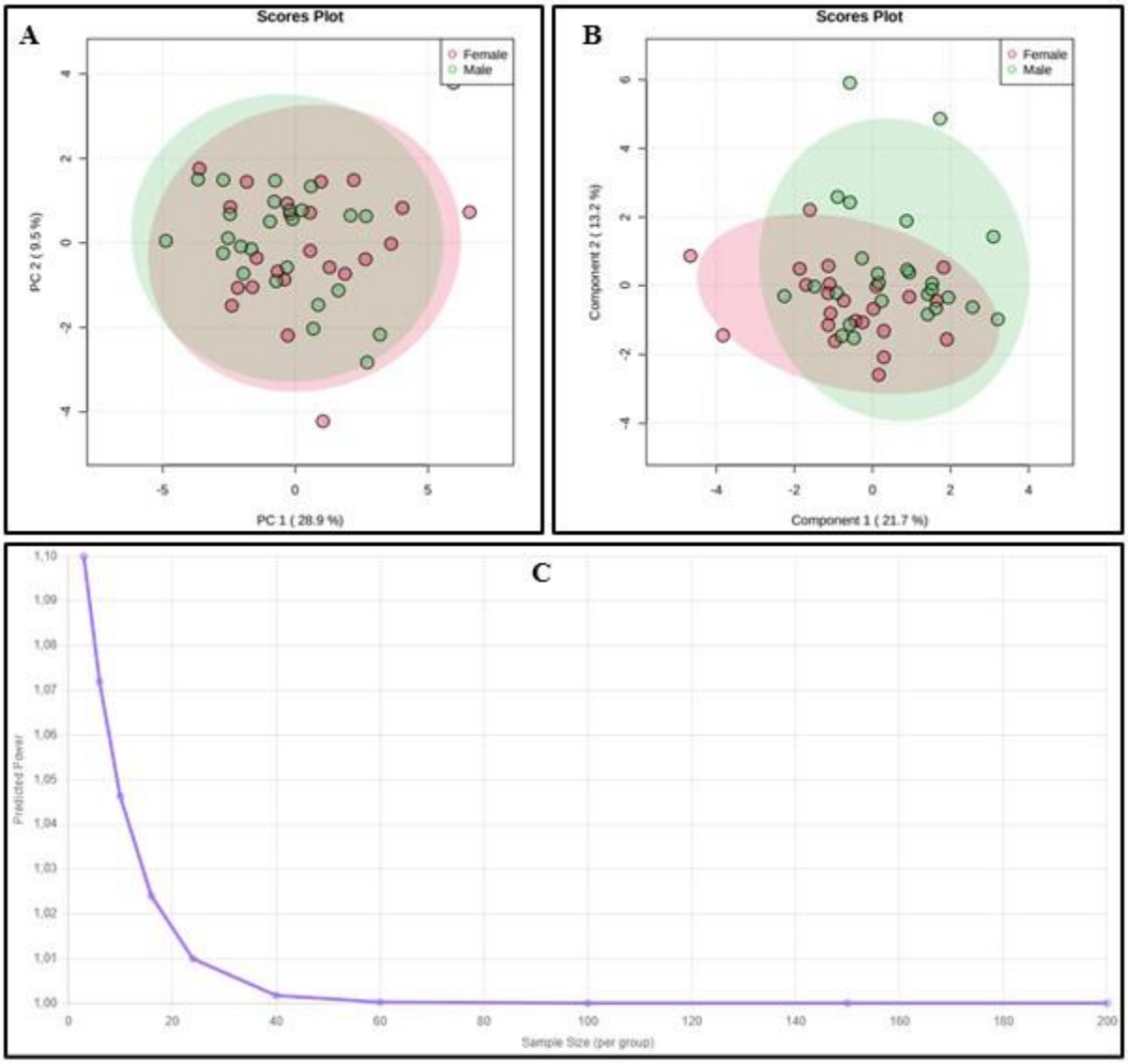


**Figure 3.1.2**. Discrimination analysis of gender in *M. glacialis* concerning biometric parameters: principal component analysis (**A**), and partial-least square discriminant analysis (**B)** (with $R^2$= 0.3 and $Q^2$= - 0.4); and predictive power analysis (**C**) of the statistical model quality. N= 23 females and 26 males.

## Sex and biometric measures do not influence CFF total protein quantification in non-regenerating starfish

CFF total protein concentration was determined in 31 individuals, to access sex differences in non-regenerating sea stars, through the BCA assay (see attachment 3). This technique measures the quantity of proteins of a given alkaline solution by measuring the formation of $Cu^{+}$ from $Cu^{2+}$ by the Biuret complex in the solution using bicinchoninic acid [68]. Sex differences are rarely studied in echinoderms, although it is important to determine the sex of individuals and their dissimilarities since gender and reproduction affect other physiological characteristics, such as the components and activities of the IS in marine invertebrates [69-70]. In the clam *Ruditapes philippinarum*, females display more abundancy of bigger hemocytes, especially in granulocytes, higher endocytic activity, and stronger lysozyme activity in the cell-free hemolymph than males [69]. In the topshell *Trochus histrio*, the increase in temperature of the seawater provides different physiological strategies between males and females, such as lipid peroxidation, heat-shock response, and antioxidant enzymatic activities [70]. Gender in sea urchin *Paracentrotus lividus* potentiates different IS activity in both cellular (tissue) and humoral (CF) responses due to a higher number of coelomocytes in females [71]. In the sea cucumber *Apostichopus japonicus*, differences in transcriptomics of coelomocytes, enzyme activities, and proteomics in the CFF were evident [72-74]. Jiang and colleagues studied the proteins variations on the CFF before and after spawning [74]. They found an increase in the protein expression of the alternative complement pathway in both females and males after spawning, meaning that the reproduction activity and breeding season also have an impact on the sea cucumber humoral immunity. Gender also affects metabolism as means to achieve reproductive success [74]. However, it was reported that variability in hemolysis activity in *M. glacialis* does not appear to be linked to sex [75]. Even though, this type of CFF activity was tested against vertebrate erythrocytes and restrictive to one of the several immunity pathways. In accordance with this evidence, this study was not found significant differences in CFF total protein concentration between non-regenerating females and males (p-value=0,07), although this could be also the result of a non-sufficient sample size since the statistical value was very low.

Also, the correlation between the biometric measures and the total protein quantification was evaluated, without the influence of sex. In this study, the non-regenerating specimens do not show this relation, since W, xAl, xAw and CDd, or even the proportions between these measures, do not appear to have an influence on the concentration of proteins circulating in the CFF (**Table 3.1.5**).

**Table 3.1.5-** Correlation test between CFF total protein concentration and biometric measures, **Al1**- length of arm 1; **Al2**- length of arm 2; **Al3**- length of arm 3; **Al4**- length of arm 4; **Al5**- length of arm 5; **Aw1**- width of arm 1; **Aw2**- width of arm 2; **Aw3**- width of arm 3; **Aw4**- width of arm 4; **Aw5**- width of arm 5; **CDd**- central disk diameter; **xAl**- mean arm´s length; **xAw** mean arm´s width; **W**- weight; and the proportions of **xAw/xAl**, **xAl/W**, **xAw/W**, **CDd/xAl**, **xAw/CDd** and **CDd/W**. Spearman coefficient of correlation and result of the test (**P-value**). N=39.

| Biometric Parameters | Coefficient of Correlation | P-value |
|---|---|---|
| ***Al1*** | 0.187 | 0.256 |
| ***Al2*** | 0.011 | 0.946 |
| ***Al3*** | 0.071 | 0.668 |
| ***Al4*** | 0.272 | 0.094 |
| ***Al5*** | 0.189 | 0.250 |
| ***Aw1*** | 0.256 | 0.116 |
| ***Aw2*** | 0.070 | 0.673 |
| ***Aw3*** | 0.112 | 0.497 |
| ***Aw4*** | 0.081 | 0.623 |
| ***Aw5*** | 0.028 | 0.865 |
| ***CDd*** | 0.271 | 0.095 |
| ***xAl*** | 0.135 | 0.413 |
| ***xAw*** | 0.005 | 0.978 |
| ***W*** | 0.076 | 0.647 |
| ***xAw/xAl*** | 0.176 | 0.288 |
| ***xAl/W*** | 0.034 | 0.836 |
| ***CDd/xAl*** | 0.193 | 0.238 |
| ***xAw/CDd*** | 0.107 | 0.519 |
| ***CDd/W*** | 0.097 | 0.557 |

# 3.2. Differentiation Features within Coelomocytes Populations in Non-regenerating Conditions

IFC is a powerful technique that combines FC with fluorescence microscopy allowing multiparametric fluorescence and morphologic analysis of thousands of cellular events according to their real images. To easily discriminate subpopulations of the CF cellular populations of starfish through morphologic features in future experiments resorting to IFC. This study is presented a brief morphologic discrimination of the coelomocytes morphotypes circulating in non-regenerating *M. glacialis* starfish.

P1 and P2 cells differ significantly in complexity and in the cell area, in which P2 cells displayed a greater cell structural complexity and high variation in cell size, ranging between 100 to 500 $mm^2$ of area, while P1 cells are smaller, with areas values ranging from 50 to 130 $mm^2$ [45], facilitating the visual distinction of these two populations. It is evident the existence of two subpopulations in the cell population P1, where it seems that the P1L cell type, since displayes a higher nucleus/cytoplasm ratio and low mitotic activity, corresponds to a nondifferentiated form of the more mature undifferentiated P1S cell type [45]. This P1L cell mentioned already in the coelomic epithelium in starfish *Asterias Rubens* [76], could be the progenitor of the circulating cells [45]. Based on the assumption the greater the RD mean value, the greater the morphologic difference between two cell types. P1S and P1L seem to be very different in the bright detailed intensity (the intensity of the pixels in the bright detail image) feature (**Table 3.2.1**), when analyzed in the bright field channel. Moreover, the relation between this feature with background mean (average intensity of the background of the cell image) (**Table 3.2.1**) results in almost fullest separation of these morphotypes (**Figure 3.2.1**), meaning that these cells have notable differences in terms of texture. The P1S cells display a wide range of background mean and greater bright detailed intensity values compared to P1L cells (**Figure 3.2.1**).

**Table 3.2.1.** Morphologic discrimination through the best discriminator features of the P1 morphotypes of *M. glacialis.* **RD mean**- Risk Difference mean.

| Cellular morphotypes | Discriminator feature | RD mean |
|---|---|---|
| **P1S and P1L** | Bright detailed intensity | 1.23 |
| | Background mean | 0.83 |
| **P1S and P1B** | Standard deviation of the object | 1.54 |
| | Modulation | 1.13 |
| **P1L and P1B** | Standard deviation of the object | 2.62 |
| | Modulation | 2.30 |

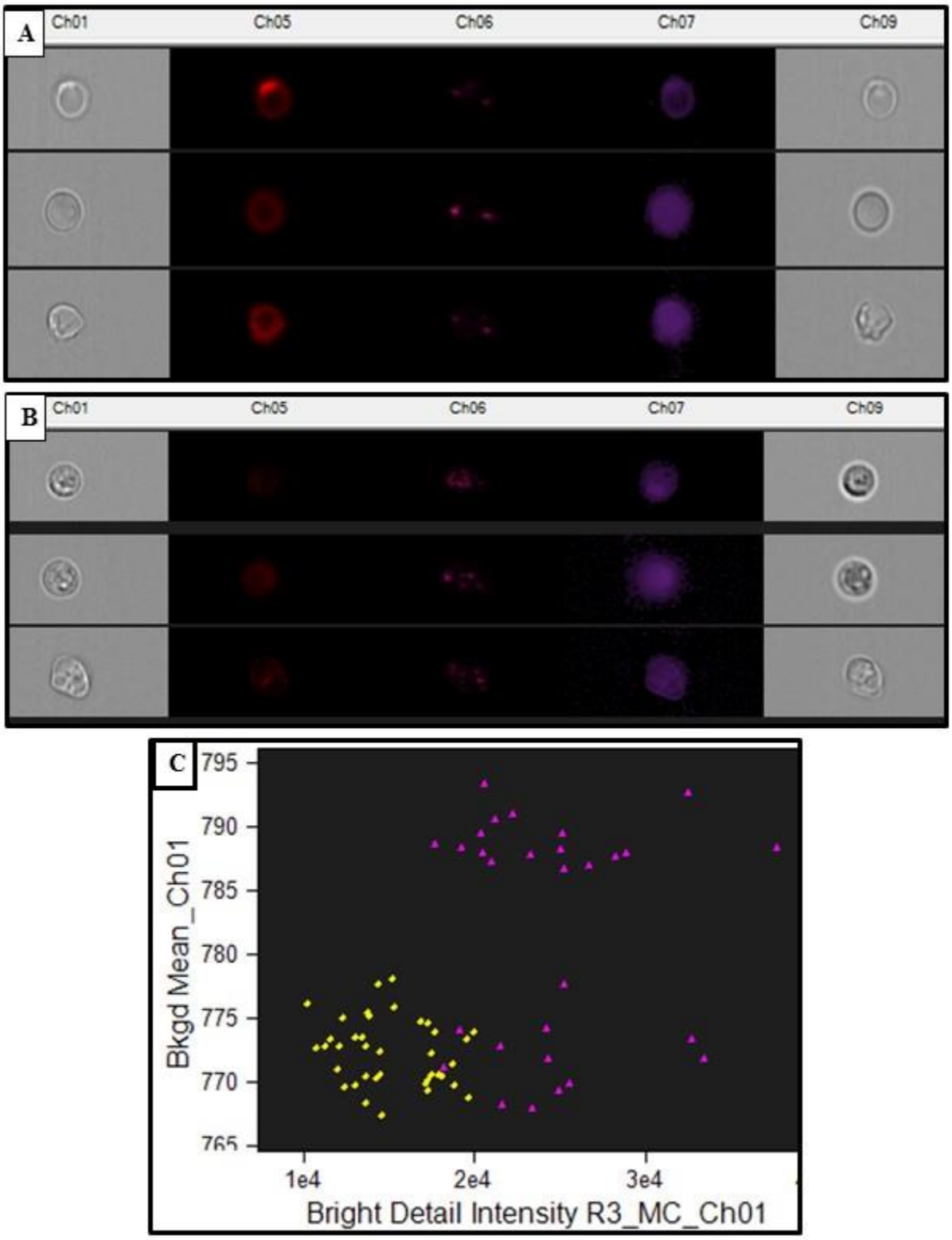


**Figure 3.2.1.** Differentiation between P1S **(A)** and P1L **(B)** cells trough the texture parameters of background mean and bright detail intensity **(C). A** and **B** are representations of images or signals detected by side scatters (channels 1 and 6), bright field (channel 1 and 9), FM 4-64 marker (channel 5), and DAPI (channel 7). Yellow diamond- P1L; purple triangle- P1S.

Here, a new cell type of the population P1 (designated here as P1B- P1 brighter cell) is separated in a single different subpopulation from the other two cell types. P1B cell shows morphologically a strong brightness in white outside the cytoplasmatic membrane and in black inside the cell, or vice-versa, in the images of bright field and SSC channels (**Figure 3.3.2 A**). This cell type also differs from the P1L and the P1S cells in terms of texture, especially in standard deviation (describes the overall distribution of pixel intensities) and modulation (measure of the intensity range of an image) parameters, displaying greater values than these two morphotypes (**Table 3.2.1**, and **Figure 3.3.2 B** and **C**).

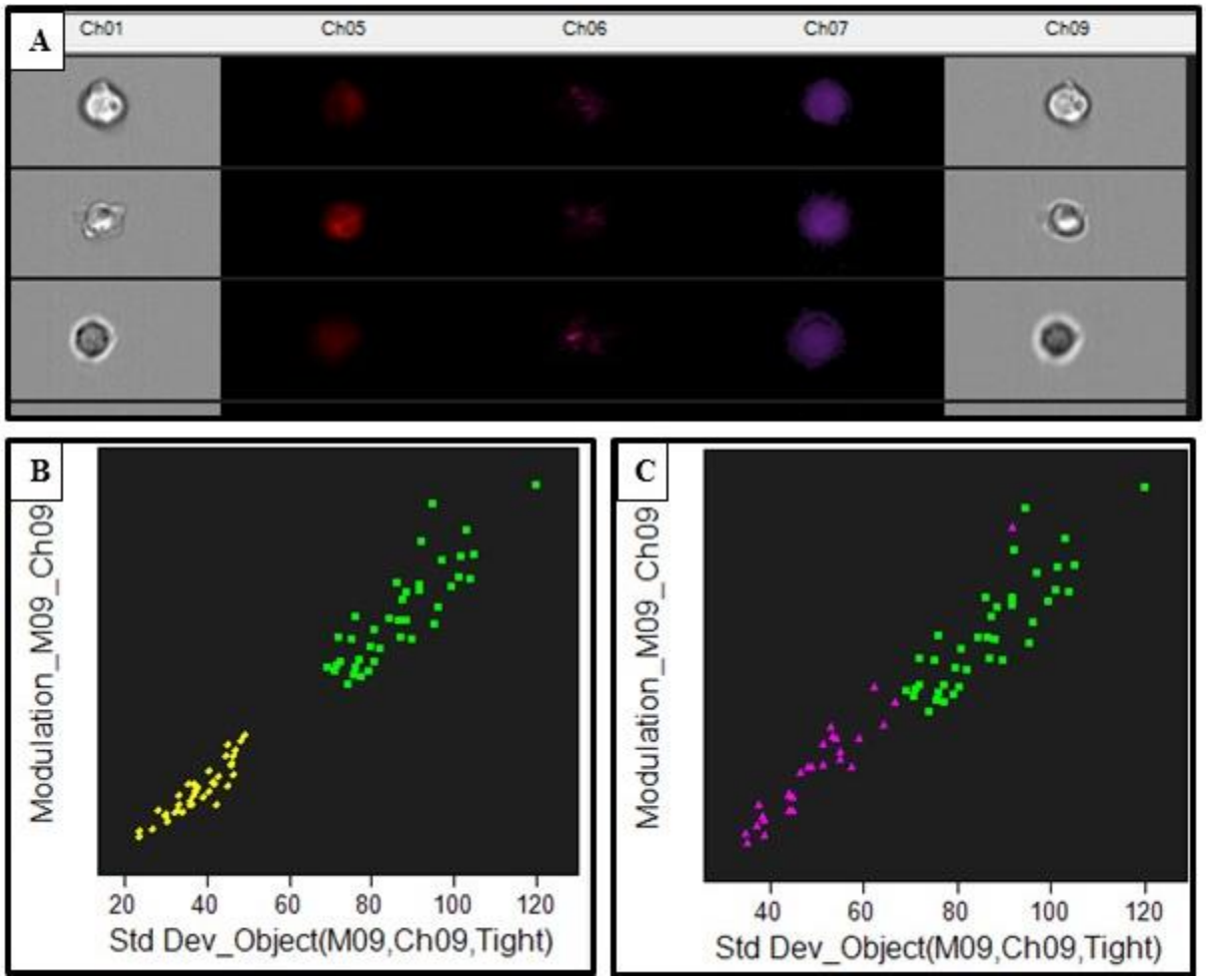


**Figure 3.2.2.** Differentiation between P1B (**A**), with P1S (**B**) and P1L (**C**) cells through the texture parameters of modulation and standard deviation object**. A** is a representation of images or signals detected by side scatters (channels 1 and 6), bright field (channel 1 and 9), FM 4-64 marker (channel 5), and DAPI (channel 7). Yellow diamod- P1L; green square- P1N; purple triangle- P1S.

Regarding the population P2, as expected, the distinction between phagocytes (**Figure 3.2.3. A** and **B**) and between thrombocytes (**Figure 3.2.3 C** and **D**) presented fewer RD mean values than between each other (**Table 3.2.2**).

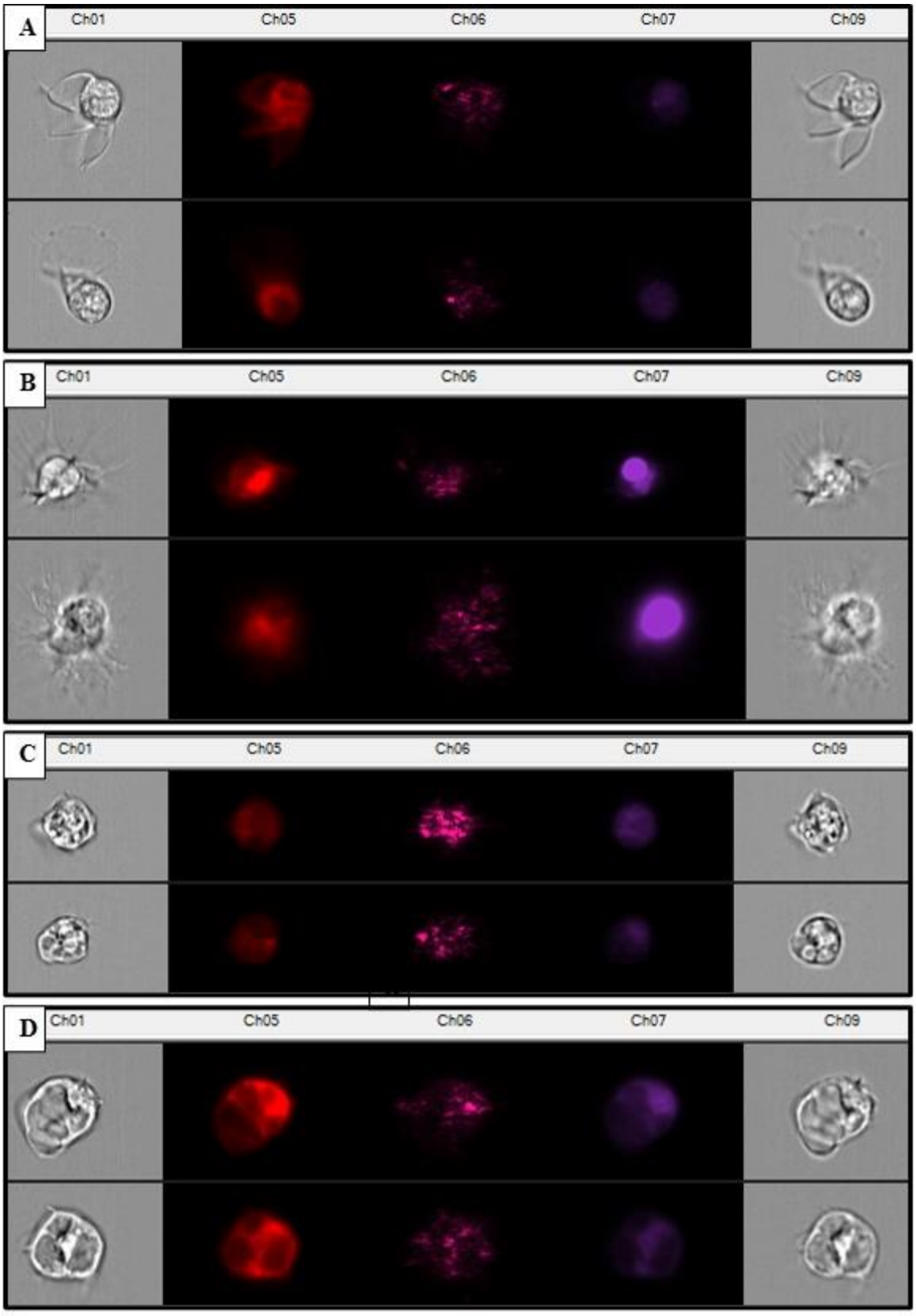


**Figure 3.2.3.** Representation of images or signals of petaloid (**A**), filopodial (**B**), big granulated (**C**), and polygonal (**D**) cells, detected by side scatters (channels 1 and 6), bright field (channel 1 and 9), FM 4-64 marker (channel 5), and DAPI (channel 7).

Nonetheless, the texture is apparently the best parameter to discriminate the petaloid from the filopodial forms, through the cell modulation and bright detail intensity features (**Table 3.3.2** and **Figure 3.2.4 A**), and to determine whether the cell is big granulated or polygonal, particularly through the features of bright detail intensity and cell area (size of the cell in square microns) (**Table 3.3.2** and **Figure 3.2.4 B**). It seems that the petaloid form is relatively harder to distinguish from the thrombocytes than the filopodial form. Which can be discriminated from the regular cell through the features of size, particularly the height (based on a bounding rectangle, the height is the size of the higher side) and shape, particularly the circularity of the object (degree of the cell´s deviation from a circle) (**Table 3.2.2** and **Figure 3.2.4. C**), and from the big granulated cell through the shape, especially the shape ratio (ratio between the smaller side/width of the already mentioned rectangle and the longest part of the cell/length) and the thickness minimum (smaller width of the cell) (**Table 3.2.2** and **Figure 3.2.4. D**). While the filopodial form is different from the regular cell in the shape ratio and bright detail intensity (**Table 3.2.2** and **Figure 3.2.4. E**), and from the big granulated in thickness minimum and shape ratio (**Table 3.2.2** and **Figure 3.2.4. F**). The IFC has already proven to be efficient in the distinction of cell types through morphometrics in vertebrates, which with other techniques would not be possible to achieve [77-78]. In the Atlantic salmon *Salmo salar*, the IFC allowed distinguishing head kidney leucocytes from macrophages/monocytes populations through cell area of the bright field and SSC intensity [78]. Also, with the feature of cell area, the ImageStream allowed the discrimination of human tumor circulating cells and consequently permitted the implementation of a new way of detection of hepatocellular carcinoma [78].

**Table 3.2.2.** Morphologic discrimination through the best discriminator features of the P2 morphotypes of *M. glacialis.* **RDmean-** Risk Difference- mean.

| Cellular morphotypes | Discriminator feature | RD mean |
|---|---|---|
| **Filopodial and Petaloid** | Cell modulation | 1.04 |
| | Bright detailed intensity | 0.88 |
| **Big granulated and Regular** | Bright detailed intensity | 1.62 |
| | Cell area | 1.55 |
| **Filopodial and Regular** | Cell height | 1.56 |
| | Circularity of the object | 1.31 |
| **Filopodial and Big granulated** | Shape ratio | 1.85 |
| | Thickness | 1.66 |
| **Petaloid and Regular** | Shape ratio | 1.50 |
| | Bright detailed intensity | 1.49 |
| **Petaloid and Big granulated** | Thickness | 2.53 |
| | Shape ratio | 2.47 |

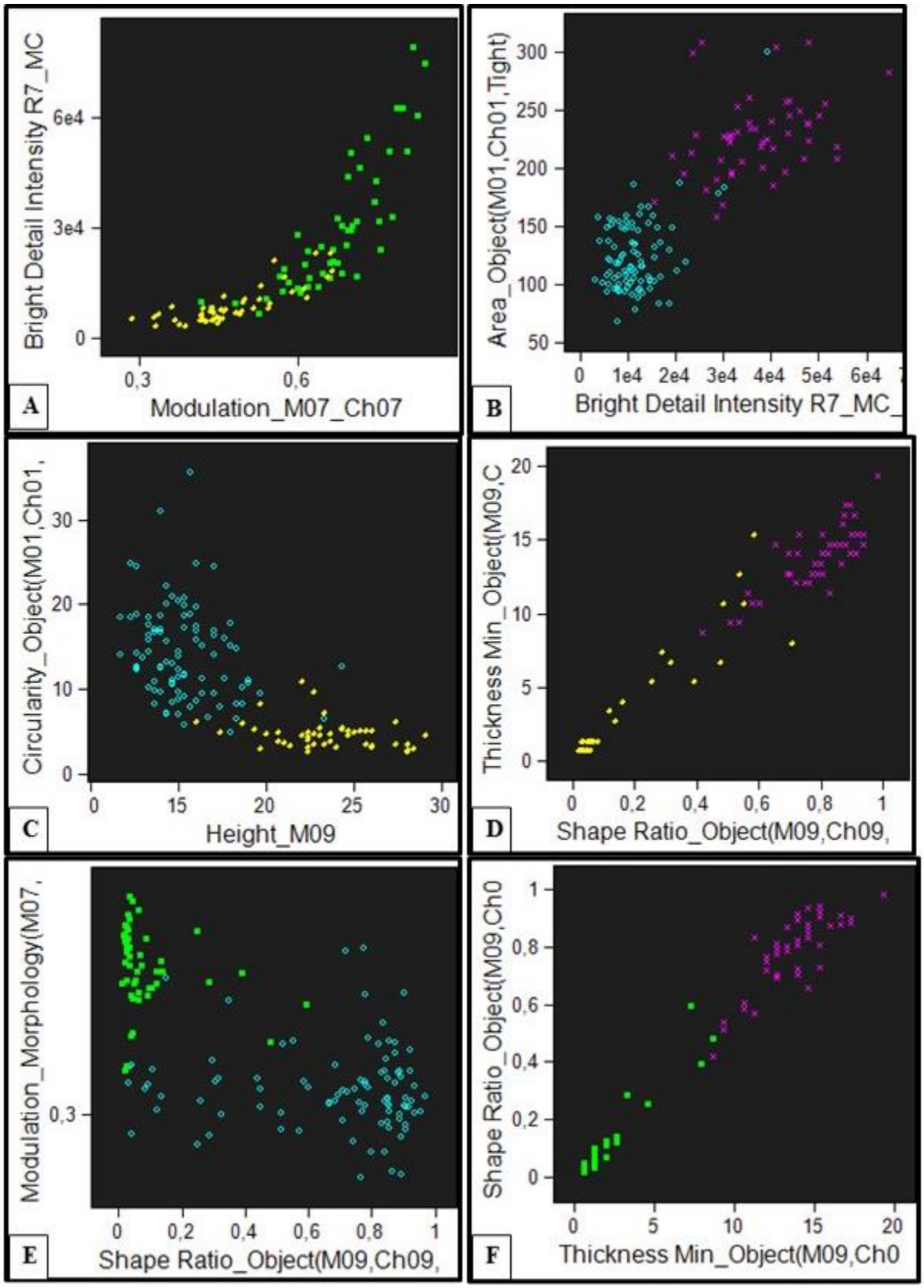


**Figure 3.2.4.** Differentiation between petaloid and filopodial cells (**A**), big granulated with polygonal cells (**B**), petaloid with polygonal (**C**), and big granulated cells (**D**), filopodial with polygonal (**E**), and big granulated cells (**F**), through the texture features of modulation and standard deviation object, the size features of cell area and height, and the shape features of circularity of the object, thickness, and shape ratio. Yellow diamond- petaloid; green square- filopodial; blue empty circle- big granulated; purple cross- polygonal.

# 3.3. Post-Traumatic Radial Nerve Cord Regeneration

The regenerative potential, or the potential for regenerating tissues, organs, and body parts, is expressed to a maximum extent in echinoderms [24]. Which have a remarkable capacity to rapidly regenerate lost tissues [47], including the RNCs [7,11]. This contrasts with mammals, especially humans, that are inefficient to replace a damaged CNS, and that possess a limited regeneration capacity, translating in a renewal of only specific tissues or a non-fully functional regrowth in this system [79-80]. Also, its repair by repopulation of stem cells at the site of injury is inefficient due to the complexity of the regulatory systems of cells, tissues, and organs in which these cells will give origin [80]. Therefore, to reach new exogenous pathways of regeneration stimulation, it is essential to understand why the regenerative process is not active in certain human systems, through the experimentation in organisms where this process occurs entirely [52,80].

## Variability in CFF protein concentration during radial nerve cord regeneration

The CF contains soluble factors, such as proteins, that are constitutively secreted or released under specific physiological conditions from different sources throughout the body. Several soluble factors are involved in different physiological processes, such as wound healing, inflammation, tissue remodeling, and cell migration. Consequently, they can serve as biomarkers of their corresponding processes and can provide a general profile of the biological state of the organism [16]. In this perspective, this study aimed to investigate the dynamics of the circulating proteins through quantification comparing the three different time-points and control resorting to the BCA assay (see Attachment 3). Through this technique was determined significant differences regarding the regenerative process, only between day 1 p.a. and day 14 p.a. (p-value=0,021). Also, the control group and the days 1 and 7 p.a. (p-value=0,007 and p-value=0,022 respectively) are significantly different in terms of CFF total protein concentration (**Figure 3.3.1**).

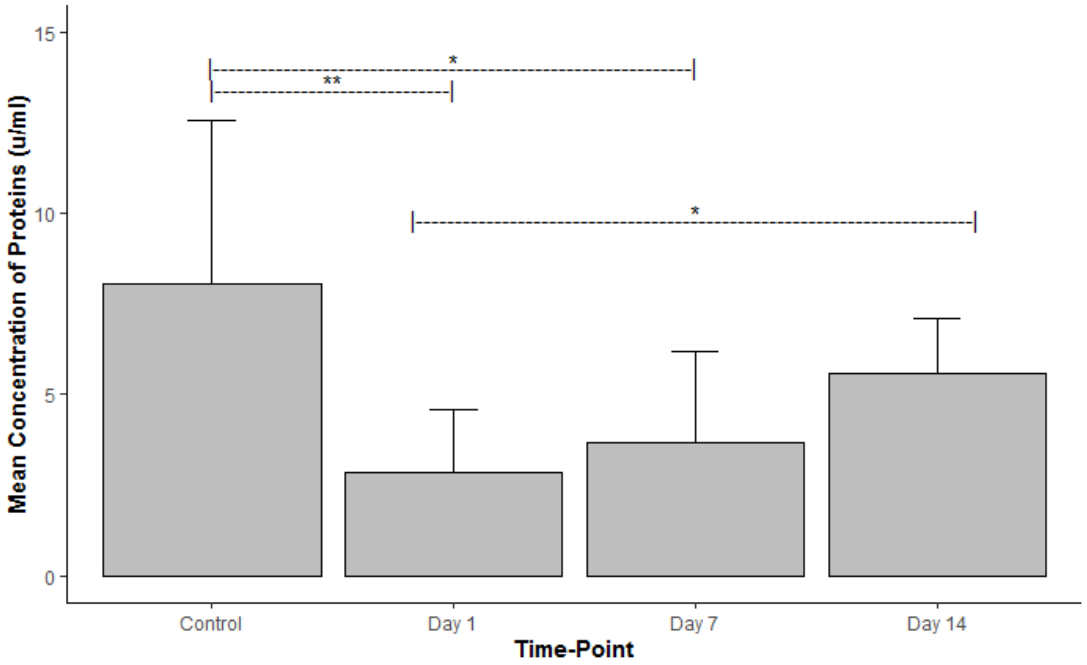


**Figure 3.3.1.** Mean concentration of proteins circulating in the coelomic fluid free of cells in the homeostatic state (control group) and at the regeneration times: 1, 7 and 14 days. N= 10 (control group), 6 (day 1), 4 (day7) and 5 (day 14). The mean concentration for the control group was determined for the total control animals, independently of the day. Note: * means p-value<0.05; ** means p-value<0.01.

Unfortunately, the quantification analysis determined a low concentration of protein which made impossible the quantification resorting to the LCMS-MS. Several high-throughput studies already characterized the *M. glacialis* proteome of various tissues in a homeostatic state, through SDS-PAGE followed by mass spectrometry [4,19,53]. In the CFF, Franco (2011) [4] identified 47 proteins, the majority playing important roles in the echinoderm immunity and proteins that may be related to intrinsic neuronal growth capacity such as tenascin (axon guidance during neuron migration, development, and neuronal regeneration). A much different number was found by Shabelnikov and colleagues [16] that identified 91 proteins in the CFF of the sea star *Asterias Rubens*. In coelomocytes proteomic characterization, 358 proteins were identified, including proteins involved in regeneration, related to the formation of the thickened wound epithelia immediately after injury [19]. Relative to the proteome of the RNC, 281 proteins were characterized, and additionally, 158 proteins were identified in the synaptosomal membranes. Additionally, were reported proteins involved in synaptic transmission, neurogenesis, regeneration, and sensory perception [53]. As expected, different tissues have different proteomes, however, in every single one was identified proteins related to regeneration. To confirm that the BCA assay results are explained by the regenerative process, the concentration of proteins before the regeneration experiment, i.e., in the non-regenerative state, was assessed for every sea star, in which the collection of the CFF occurred in two separate days for different specimens (**Figure 3.3.2**). Interestingly, the concentration was significantly different (p-value=0,047), meaning that the probable source of difference is the period where the CF was collected rather than the different periods of regeneration.

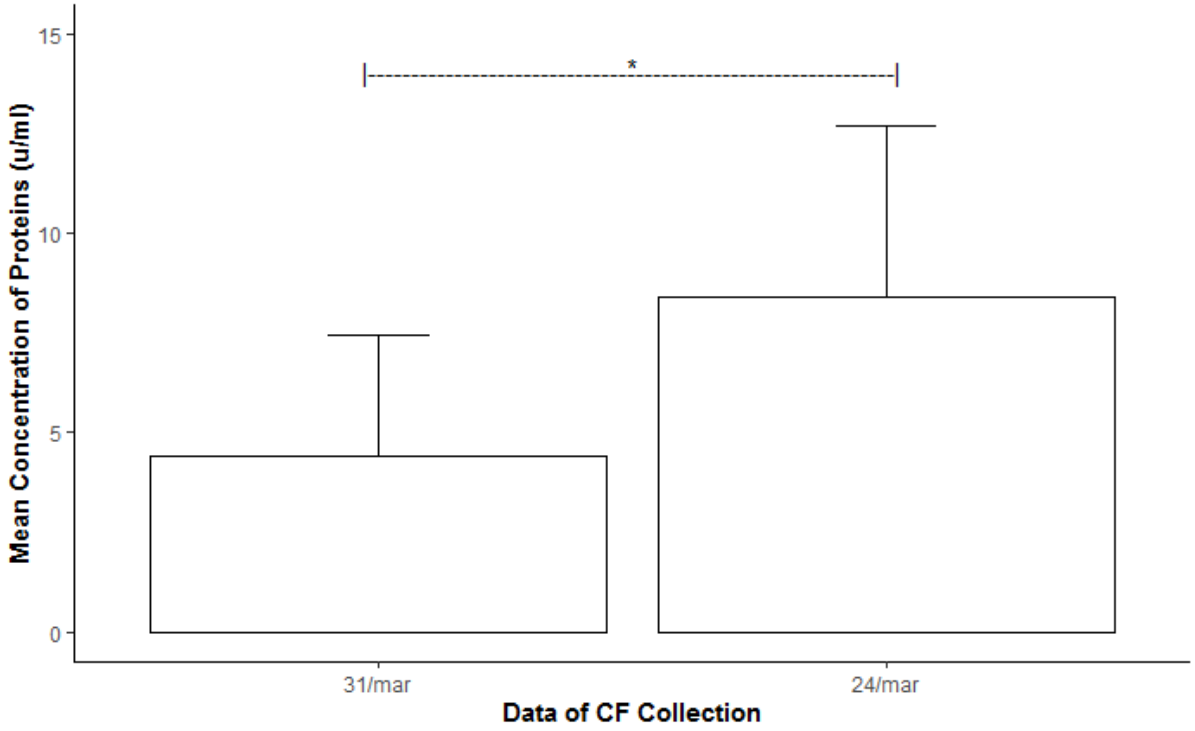


**Figure 3.3.2.** Quantification of proteins circulating in the coelomic fluid free of cells of non-regenerating animals in two different days: 24/mar and 31/mar. N= 18 (8 in 24/mar and 10 in 31/mar). Note: * means p-value<0,05.

## FC allowed the detection of a new population involved in radial nerve cord regeneration

Cellular populations of the CF of both regenerative and non-regenerative samples were characterized through FC. Since coelomocytes tend to aggregate due to their clotting functionalities, we cannot exclude that a fraction of cells was retained during the filtration process. Another issue is that cellular debris appears in the CF samples which could interfere with the correct reading and consequent disposition of coelomocytes populations in FC. Therefore, to discriminate valuable coelomocytes from cellular debris, DRAQ5, a lipophilic and membrane permeable to DNA dye that allows detecting live cells [81], was used.

Previously, populations of coelomocytes of sea stars in a non-regenerative state were characterized and subdivided into two populations through FC [45]. The P2 cells displayed higher side scatter (SSC) and forward scatter (FSC) values than P1 cells, probably due to a more complex/structured surface and richer internal cyto-architecture. As well, P2 cells incorporated approximately double the amount of DRAQ5 of P1 cells. Another evidence is that P2 cells are more abundant, representing 60-70% of coelomocytes. These features are also displayed in this study. FC analysis of the cellular portion of the CF, detected two distinct populations, with different morphological complexity and fluorescence properties, similar in every experimental group (**Figure 3.3.3** and **Figure 3.3.4**). **Figure 3.3.3** shows that population P1 displays lesser values of SSC and values of DRAQ5 incorporation than cells from the population P2, in the control group. Also, the population P2 shows higher density (on average approximately with 88% of total cells), and consequently a greater mean number of cells than P1 (on average approximately with 4% of total cells), with greater difference than in the previous study. It is important to notice that cells detected outside the limits of the two populations were not placed in a

sufficient abundance zone of the plot, to be considered another population, or were identified as aggregates of cells.

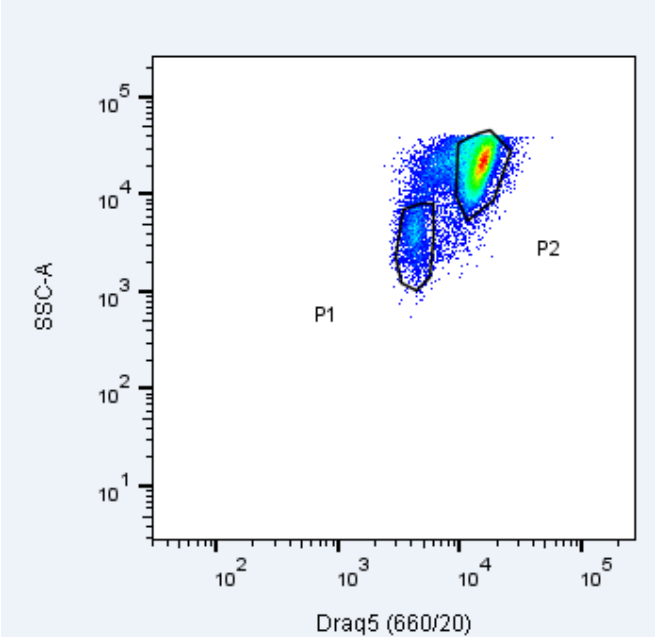


**Figure 3.3.3.** Flow cytometry analysis of a typical dot plot of circulating coelomocytes stained with DRAQ5 of 6 non-regenerating individuals.

In respect of the regenerative process, **Figure 3.3.5** shows that a new population, designated here as P3, appears gradually along the regeneration time. On day 1 of regeneration, only the two populations P1 and P2 could be distinguished. On day 7, a new population appears with a significant number of cells to be considered a different population. Finally, on day 14, this new population displays similar characteristics but a higher density than 7 days before. In Andrade et al. (2021) [45], a new type of coelomocyte, similar to polygonal phagocytes, was visualized through fluorescence microscopy. Which curiously, appeared at 7 and 14 days post-traumatic regeneration of the RNC in *M. glacialis* (results not published). This cell type is characterized by having a concentrated granular region that hosts the nucleus, surrounded by a homogenous cytoplasm extending into an elongated filopodium (**Figure 3.3.4**) [45].

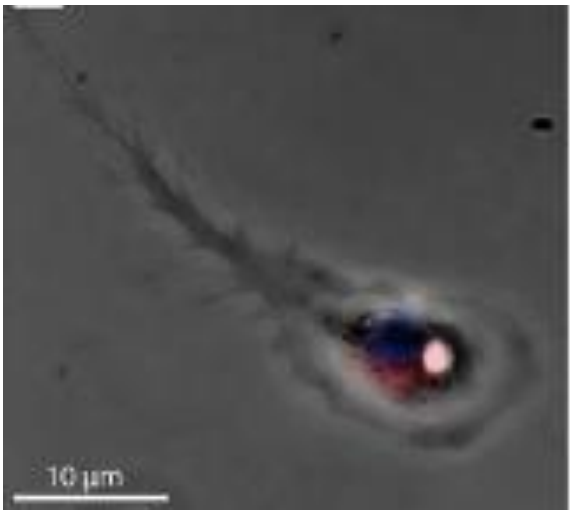


**Figure 3.3.4.** P2 coelomocyte morphotype detected by fluorescence microscopy in the CF of *M. glacialis*. Adapted from [45].

Moreover, P3 cells appear to display similar DRAQ 5 incorporations of P2 cells, however apparently with side scatter values similar to those of P1 cells (**Figure 3.3.5**), suggesting some morphologic characteristics with this cell type.

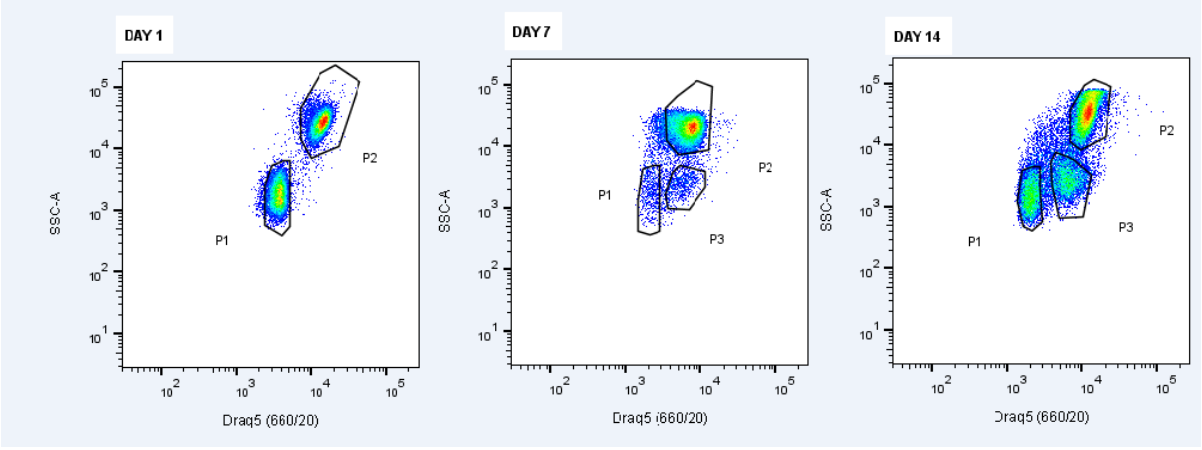


**Figure 3.3.5.** Coelomocytes flow cytometry analysis during Radial Nerve Cord (RNC) regenerative process. Typical dot plots of circulating coelomocytes stained with DRAQ5 at days 1, 7 and 14 after partial nerve excision. N=5 per time-point.

Regarding the existence of strong evidence that P3 cells participate in the RNC regenerative process, their function is not known, and the origin of these cells can only be speculated. Where coelomocytes come from is still a big mystery. The axial organ [82], the Tiedemann's bodies [83], the haemal organs [84], and the perivisceral coelomic epithelium [85-87] are the candidates to be the so-called hematopoietic tissue in sea stars. The axial organ is a haemal tissue next to the stone canal (tube with calcareous deposits leading the madreporite to the WVS) that connects the oral and the aboral haemal rings [84]. This organ is thought to be an ancestral immune organ, where the immune cells respond to an exterior stimulation with antigens in this organ, by means of cellular and humoral

immunity. The cells from this organ were subdivided into two subpopulations, possibly in the immune cells already known to circulate in the CF [82]. The Tiedemann´s bodies are small irregularly shaped vesicles situated in the ring canal of the WVS. Since this organ is bath by the major fluid systems of the organism, its cells have the capacity to perform endocytosis of bacteria and are constituted by cells similar to coelomocytes, it may function as primitive lymphoid tissue [83]. Moreover, in the Tiedemann´s bodies, the axial organ and the haemal organs was detected the formation of new cells through the radiation of the nuclei after the incorporation of H3-thymidine, which undergoes DNA replication [84]. However, this process occurred with a smaller ratio than in other tissues, particularly compared with the epithelial tissue of the tube feet, and do not specify which cells are being formed, seeming unlikely that their primary function is the formation of new coelomocytes [87]. For this reason, the most accepted organ to be the putative hematopoietic tissues is the coelomic epithelium. After stimulation with immune-stimulating molecules, the coelomic epithelium experienced a pronounced cell proliferation with an increase in the number of coelomocytes [86]. Indeed, in the CE were identified by histology and immunofluorescent staining small undifferentiated cells with a high nuclear-cytoplasmic ratio that are capable to migrate into the CF [76]. Another contribution to support this theory is the existence of marginal coelomocytes at the surface of the coelomic epithelium that may serve as a reserve pool of the circulating cells [85]. A possible explanation for the appearance of this new population of cells is the hypothesis made recently for the source of the cells involved in arm tip regeneration of sea stars [88]. The authors claim that the regeneration is made through undifferentiated stem/progenitor cells coming from distant different sources, like the coelomic epithelium, rather than through differentiated cells. Consequently, these cells act in four-step as follows: 1) hound healing by coelomocytes; 2) migration of distant progenitor cells of mixed origin; 3) proliferation of these cells in the regenerative organ; 4) local proliferation. Nonetheless, it is important to characterize from the simplest undifferentiated cell to the most complex cells that flow in the CF.

The proportion of cell events of each population detected in the regenerative and non-regenerative samples of CF was determined by FC (see Attachment 3). P1 and P2 cells do not show significant differences between each population with the time of regeneration and between each time-point and the control group (**Figure 3.3.6 A** and **B**). In turn, P3 has a significantly higher density on day 14 than on day 1, and than the control group, without significant difference with day 7 (P-value < 0,05). Also, P3 has a higher density on day 7 than on day 1, and than the control group (**Figure 3.3.6 C**). Few control samples also had a lower number of cells with equal P3 cell values. Posteriorly to the arm amputation, sea stars performed self-autotomy of the arm and the CF was collected in the adjacent arm and was examined through FC. It was evident that 66 days after the autotomy the P3 cells persisted in circulation throughout the coelomic cavity in the sea stars of the $14^{th}$ day p.a., which was not visualized in the control group (unpublished work), evidencing the participation of these cells in the regeneration process.

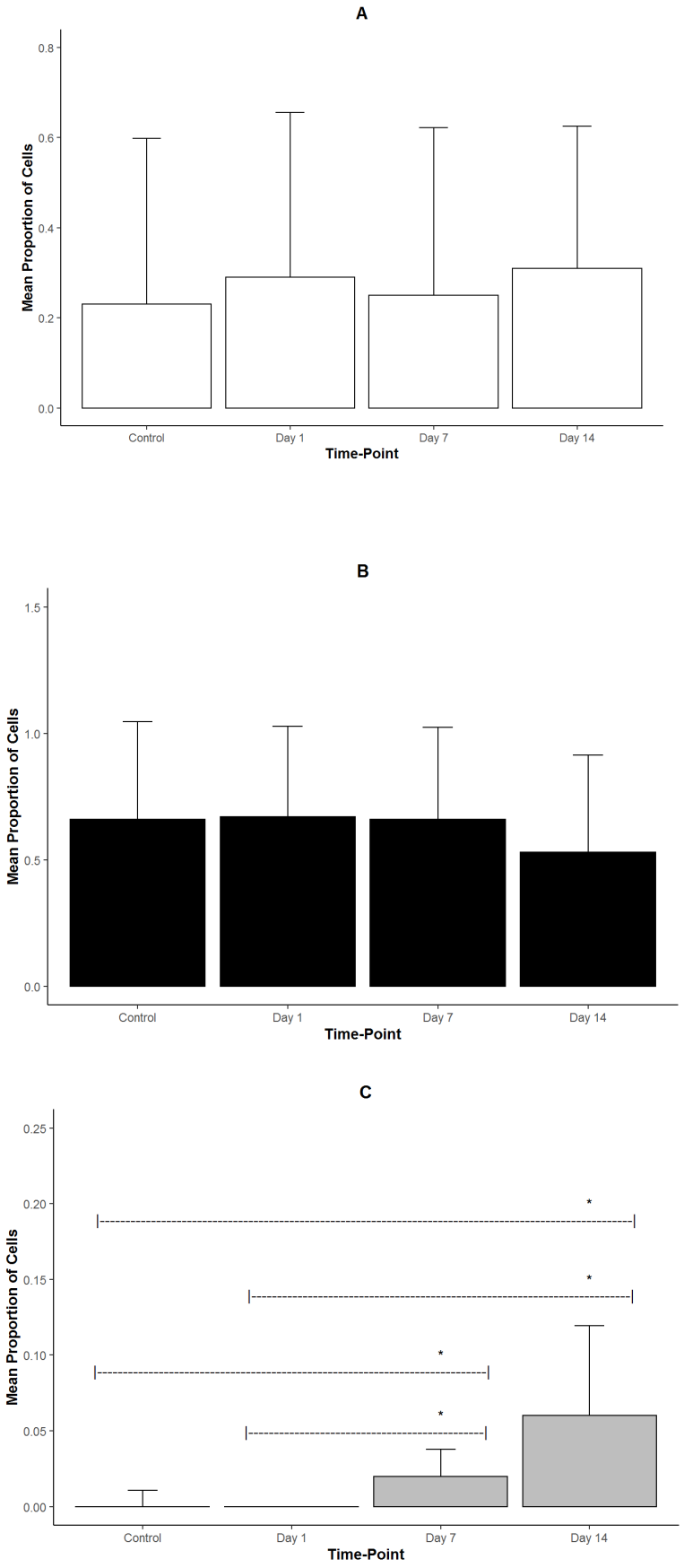


**Figure 3.3.6.** Bar plots of the mean proportion of P1 (**A**), P2 (**B**) and new P3 (**C**) cells in control and in each time-point (1, 7 and 14 days) of the radial nerve regeneration. N=21 (6 controls and 5 in each time-point). Note: * means p-value<0,05.

## Cellular and tissue patterns involved in the RNC regeneration are consistent with arm tip regeneration in starfish

Under the light of the histology tools, the RNC tissue and cellular patterns, as well the neighboring tissues, were accessed through light microscopy for morphological characterization of the RNC p.a. regeneration, resorting to the trichromatic coloration method. The trichromatic coloration allows to visualize, identify, and differentiate different tissues and structures, such as the epithelial and muscular tissues that are stained violet by the acid fuchsin, and the connective tissues, especially the collagen fibers, that are stained green by the Fast Green. Anatomically speaking, on the aboral side of *M. glacialis*, three rows of spines surrounded by pedicellariae are present outside the body wall. In the coelomic cavity, another structure that takes part of the endoskeleton emerges from the ossicles, the papullae. On the body wall, a thin external cuticle covers the epidermal layer, appearing the violet color (**Figure 3.3.7**), which is formed by flagellated cells, glandular cells, and neurosensory cells connected to the nerve plexus. Then, the above dermal layer, displayed in green (**Figure 3.3.7**), is formed by two connective tissue layers, the external loose connective tissue (LCT) and the inner dense connective tissue (DCT), and longitudinal muscle fibers. The LCT is composed of loose collagen fibers and the DCT is formed by thicker fibers mainly orientated longitudinally. The DCT in hosts calcareous ossicles which, serially repeated along the arm, form the inner supporting skeleton, that starts from the central part of the aboral body wall and moves toward the ambulacral groove. Sea stars have extensive networks of coelomic cavities that allow communication between different organs in every single part of the body. The tissue that covers the coelomic cavities is the CE. The CE is formed by a first layer of myocytes organized longitudinally and a deeper layer of myocytes organized circularly, separated by a thin layer of connective tissue, and by glandular and neural elements. Above the HS is present serious of transversal ambulacral muscles, and below appears externally the RNC, displaying the violet color derived from the epithelial tissue, running longitudinally between the rows of the ambulacral feet (**Figure 3.3.7**). [10,89]

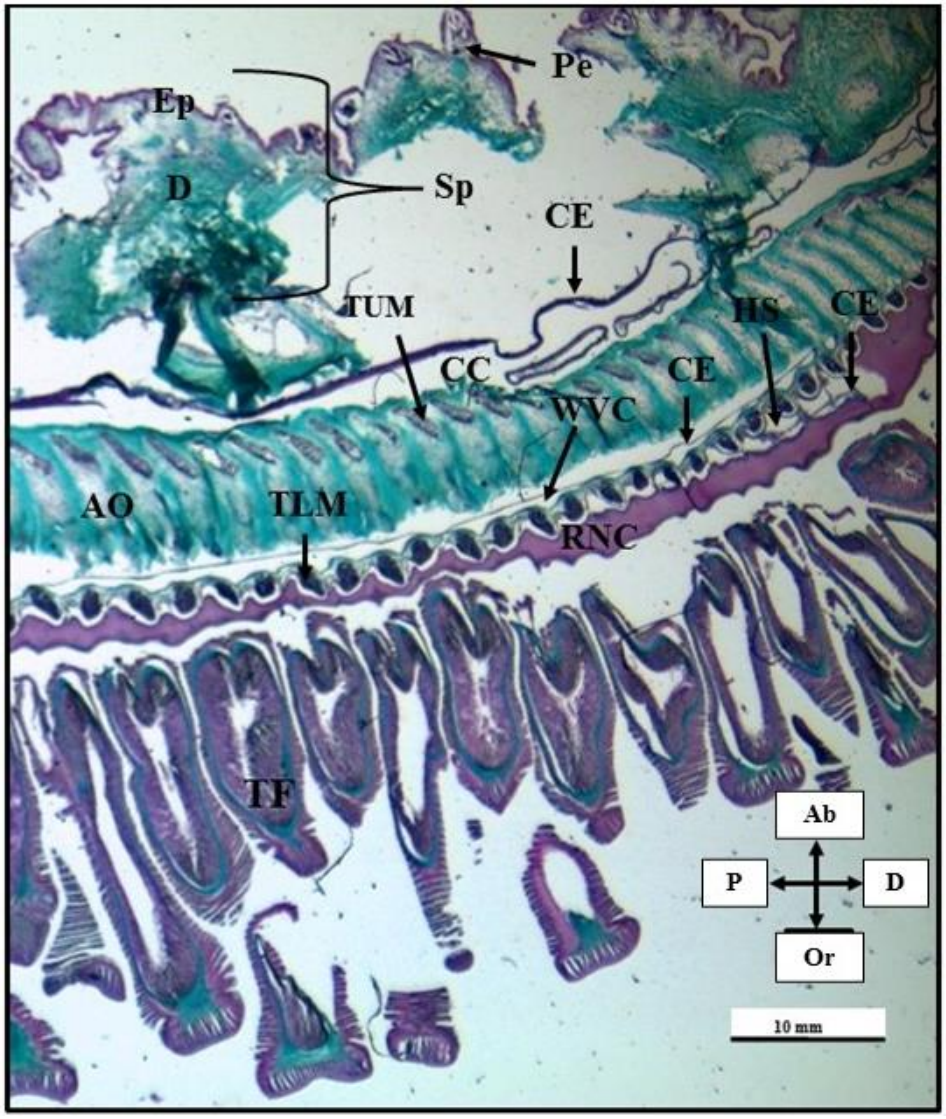


**Figure 3.3.7.** Proximal section at the sagittal plane of a non-regenerative sea star *M. glacialis*. Orientation: **P**- proximal; **D**- distal; **Ab**- aboral side; **Or**- oral side. Identification: **AO**- ambulacral ossicle; **CC**- coelomic cavity; **CE**- coelomic epithelium; **D**- dermis; **Ep**- epidermis; **HS**- hyponeural sinus; **Pe**- pedicellariae; **RNC**- radial nerve cord; **Sp**- spine; **TF**- tube foot; **TLM**- transversal lower muscle; **TUM**- transversal upper muscle.

The RNC appears to have a similar composition, morphology, and structure to other reported asteroid species [89], in which the RNC is displayed in a V-shaped, its continuous in its lateral sides with the epidermis, and the main component is the ectoneural system. This system is separated from the hyponeural system by a thin connective tissue layer (represented in blue color) (**Figure 3.3.8**). It is composed of three layers: 1) an opaque and thin hyaline layer covering the surface of the cells; 2) the somatic zone constituted by the cellular bodies of the epithelial supporting cells and the neurons, displaying a stronger violet; 3) the neuropile, a fibrillar zone constituted by neurofibrillae intermixed with the axial parts of the supporting cells, containing intermediate filament bundles, showed with a brighter violet (**Figure 3.3.8**).

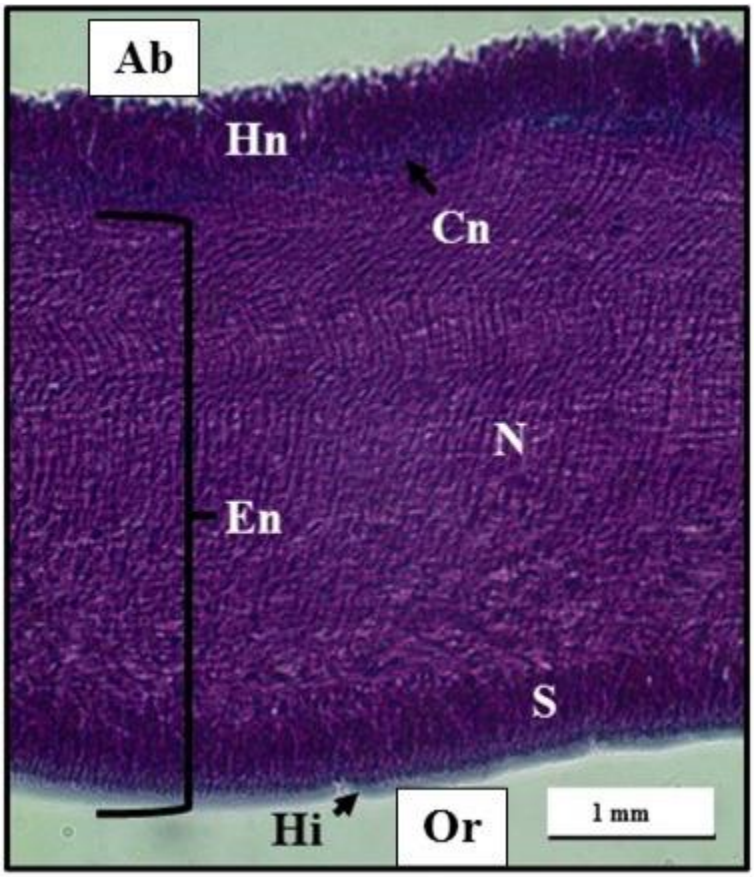


**Figure 3.3.8.** Section of the radial nerve cord (RNC), which is composed by: **Hn**- hyponeural; **Cn**- connective tissue; **En**- ectoneural, which is formed by: **N**- neuropile; **S**- somatic zone (cell body layer); and **Hi**- hyaline layer. Orientation: **Ab**- aboral side; **Or**- oral side.

In this study, the RNC showed a gradual changing morphology, as well as certain surrounding tissues, with a gain of nerve tissue to it is almost normal size in the amputation zone, over the period of regeneration (**Figure 3.3.9**). In the portion of the missing tissue or in the new tissue, the tube feet were contracted as opposed to the relaxed tube feet presented in the non-regenerative portion, which goes from day 1 to day 14 (**Figure 3.3.9**). This could be a behavioral result of the sea stars at the time of amputation, and presumably a defense reaction to protect the wound and/or the loss of the tissue function derived from the damage of motor and sensory control by the nerve. Additionally, this is a specific visual characteristic of the gap in the nerve.

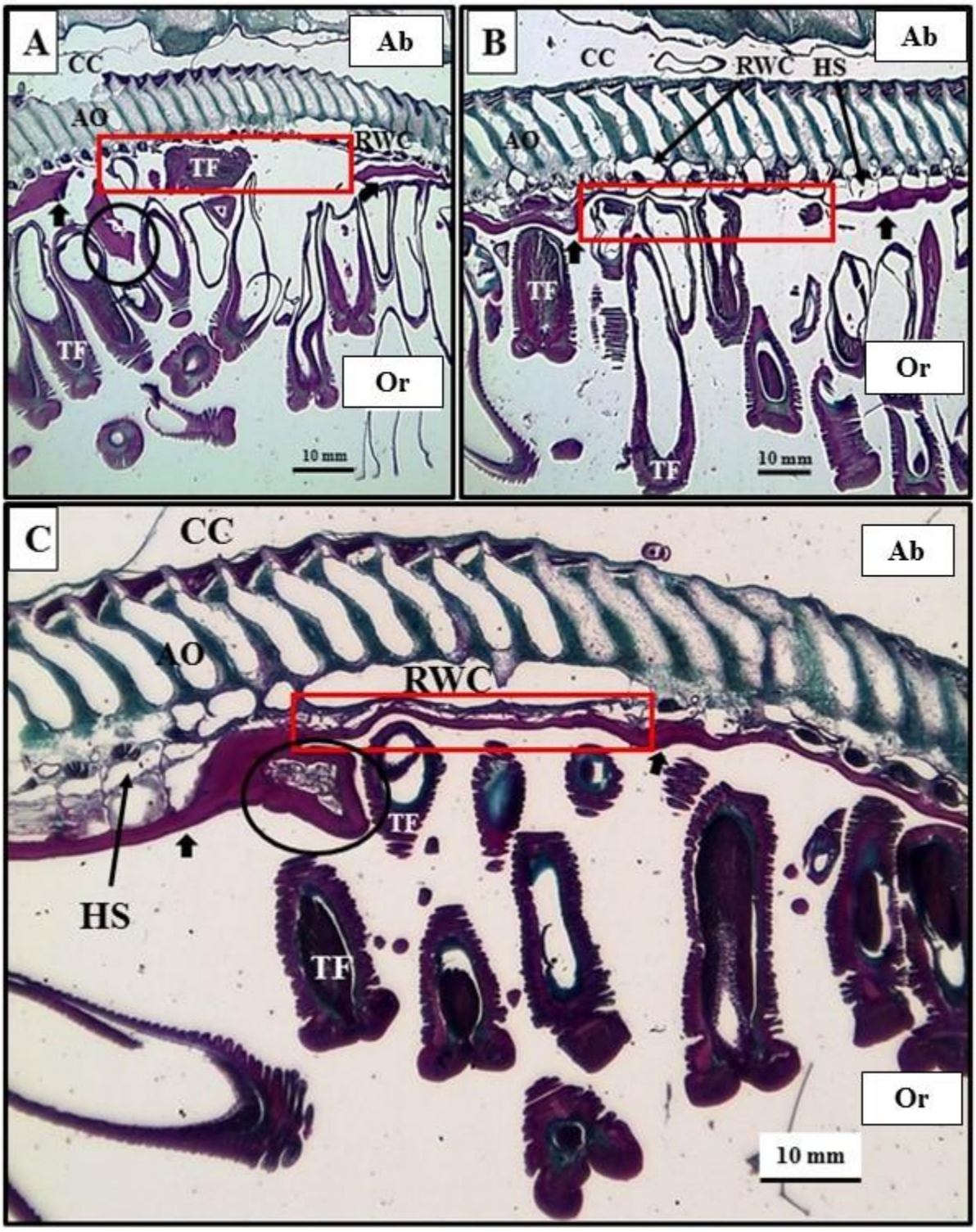


**Figure 3.3.9.** Transversal section of the regenerative arms from the period of regeneration of: (**A)** 1 day, (**B**) 7 days, (**C**) 14 days. Representation of the radial nerve cord: (arrows) the non-regenerative end, and (square) the gap/regenerative tissue.; **AO**- ambulacral ossicle; **CC**- coelomic cavity; **HS**- hyponeural sinus; **RWC**- radial water canal; **TF**- tube feet. Orientation: **Ab**- aboral side; **Or**- oral side.

On day 1 p.a, was possible to visualize in most of the samples, an incomplete RNC missing a small section correspondent to the plane of amputation. One interesting feature that was evident compared with the control samples, is the small hypertrophy of the HS and of the RWC appearing in some samples (**Figure 3.3.10 A**). One or both ends of the missing section appeared a rounded form, possibly forming a lump. At the end of this lump, the tissue is already healed, presenting the hyaline layer secreted by the glial cells, although displaying disorganization of the nerve tissue structure (**Figure 3.3.10 A**).

On day 7 p.a, contrasting with day 1, in most of the samples sectioned the nerve was no longer incomplete (**Figure 3.3.10 B** and **Figure 3.3.10 B**). Displaying in the gap a very thin nerve tissue, contrasting with a thick RNC at the proximal part and at the tip of the arm (**Figure 3.3.10 B** and **D**). This thin tissue is characterized by layers of the cellular bodies in the ectoneural epithelium and the hyponeural epithelium almost totally formed. It was often not possible to visualize the neuropile, but in some samples, a very fine line of this nerve net was already evident. Compared with day 1, on day 7, the hypertrophy was much visible occurring manly in the HS and the RWC, but also the haemal sinus in a few samples (**Figure 3.3.10 B**). In sea cucumbers day seven is considered the time point where the regeneration starts, with the initiation of the outgrowth and differentiation [11]. This process in *M. glacialis* seems to start much earlier in the regeneration period, however with similar paths, like for example, the somatic zone is the first one to differentiate, and only then the neuropile will be formed. Again, in sea cucumbers, the first regenerative zone is composed mainly of scattered supporting cell elements and intermixed supporting cell elements with bipolar shape, producing niches that were colonized by interspersed neurons [11]. The cellular events in this organism´s regenerating process are: 1) outgrowth of the nerve fibers from the stumps; 2) intense cellular division and apoptosis in both stumps and regenerating tissue; 3) an increase of spherule-containing cells [90]. An interesting aspect is that cell proliferation is not the main mechanism in holothurians RNC regeneration, but rather cooperation between this intensive cell division of the glial cells and the recruitment of already existing cells through migration, possible from deeper regions of the neuroepithelium [91]. Also, in some samples, the CE seems to go through a phase of re-structuration of its tissue (**Figure 3.3.10 B**), which can explain a prolific role in the RNC regeneration or is a consequence of the tissue destruction due to errors in handling the samples.

On day 14 p.a, the nerve tissue in the amputated section resembled a normal RNC tissue (**Figure 3.3.10 C** and **D**), with the neuropil being thicker and more prominent than on day 7 (**Figure 3.3.10 B** and **C**). In holothurians, was verified that within one month, the new RNC reached its full size and function, displaying a similar cellular and morphology composition of the uninjured nerve [90], with the prospect of happening the same in *M. glacialis*. Moreover, the hypertrophying of the coelomic canals was still very evident (**Figure 3.3.10**).

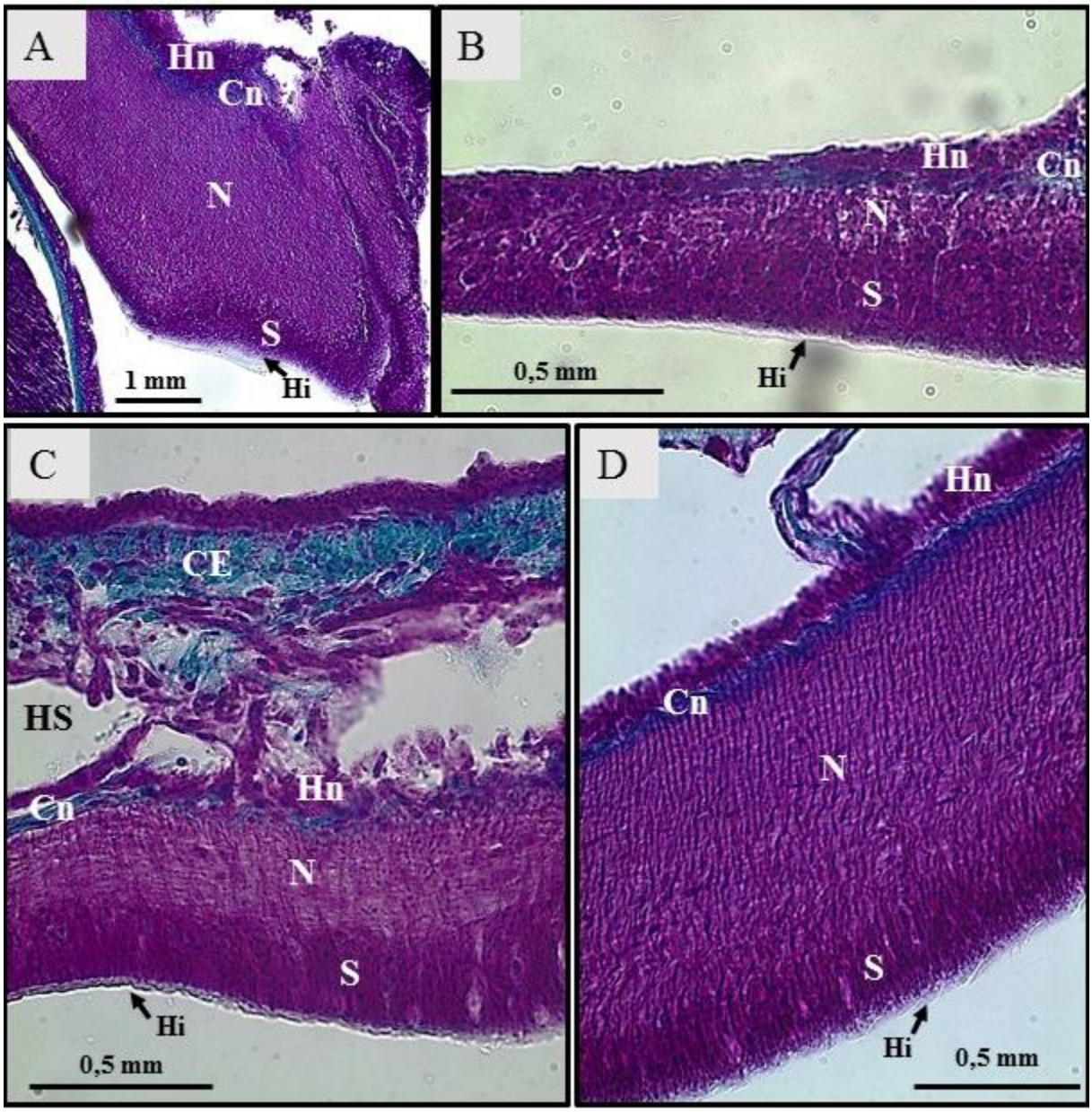


**Figure 3.3.10.** Transversal sections amplified (40x) of the regenerative arms. (**A)** Section of the clump in day 1 post-traumatic amputation of the nerve. Sections of the RNC in regeneration at 7 days p.a. (**B**) and at 14 days (**C**), and non-regenerative RNC (**D**). **CE**- coelomic epithelium; **Cn**- connective tissue; **Hi**- hyaline layer; **Hn**- hyponeural zone; **HS**- hyponeural sinus; **N**- neuropile; **S**- somatic (cell body) zone. Orientation of the figures: proximal part in the left side to distal part on the right side; aboral side at upper limit and oral side at the lower limit.

The hypertrophy of the coelomic canals could be explained by their overuse for the transportation of molecules that act in the regenerative process of the nerve. Also, could be explained by the migration of cells from the neighbor tissues or a specific niche, coinciding with the morphallaxis mechanism and with the new cells found in the cytometry results in accordance with the theory explained above [88]. According to the literature, glial cells are the primary source of progenitor cells that forms new glial and neuron cells. However, this process of cell production is insufficient for the complex process of neurogenesis, and the migration of other cells could be the complementary pathway for efficient nerve regeneration [7].

The arm tip regeneration in asteroids followed by a traumatic amputation usually involves three main phases: 1) *a repair phase*, characterized by the wound healing occurring initial migration provided by a syncytial network of phagocytes to the injury site, in order to protect the inner environment from the outer one, and first signs of neurogenesis; 2) *an early regenerative phase*, during which tissue reorganization and first signs of tissue regeneration phenomena occur; 3) *an advanced regenerative phase*, characterized by restoration and tissue regrowth with the formation of a new small regenerating arm consisting of the same structures of the adult arm [89, 92-93]. These results in RNC regeneration are consistent with studies in the arm tip regeneration in sea stars. In which the nerve tissue had a quick regeneration process, beginning with the wound healing, passing through the first signs of outgrowth and differentiation process of the neuropile and later differentiation and tissue restoration. Indeed, the time of regeneration is similar to the coelomic epithelium [10, 94-95], and to the skeleton tissues [10,94], but inferior to the muscle tissue [23].

# 4. CONCLUSIONS

This present work intended to study the sex differences in body dimensions, as well in the total CFF protein concentration, and mainly to study the cellular processes associated with RNC regeneration induced by traumatic amputation, in the starfish *M. glacialis*.

The inter-individual variability is an established fact and will continually influence the experimental investigation on sea stars. This persistence is probably due to gender, physiological status, period of the sampling collection, time of reproduction, etc. Even though, in this study, sex does not appear to influence protein concentration in the CFF of starfish in a homeostatic state. Contrasting with the day of CF collection that was demonstrated to be a factor to be accounted for in future experiments. Additionally, the size of the organism´s anatomical components, like the weight, xAl, xAw and CDd, do not appear to have an influence on the concentration of proteins circulating in the CFF, showing that they are not correlated. Moreover, these measures are not fitted to build a predictive model that discriminates between males and females of *M. glacialis* specimens, maintaining the hypothesis that these species do not have sexual dimorphism. These organisms display an enormous variability in size and weight and as expected, all these biometric parameters are correlated with each other.

In agreement with previous light microscopy, and fluorescence microscopy analysis of the CF circulating cells in non-regenerating animals. Resorting to IFC data analysis by IDEAS software, the images previously obtained of these cells [45] were subject to morphological characterization. Subpopulations of coelomocytes were successfully discriminated and characterized morphologically through texture, size, and/or shape features. Interestingly, a new subpopulation, P1B, was discriminated from P1S and P1L cell types through texture.

The regeneration study was made approaching several aspects: CFF protein quantification, coelomocytes populations by FC and regenerating RNC microscopic anatomy. It is evident that the regeneration time points show different states of the regenerative process: 1) day 1 p.a. can be considered as the wound healing phase, without any signs of regeneration; 2) day 7 p.a. an early regeneration phase is already happening; 3) day 14 p.a. the regenerative process is in the late phase. Protein quantification showed that the concentration of protein in CFF was significantly different between day 1 p.a. and day 14 p.a., and significant differences were found between the days 1 and 7 p.a. against the control group. Furthermore, as the concentration of proteins changes significantly over two different days, the regenerative process of the RNC may not influence the quantity of protein in the CFF. FC results displayed a novel coelomocyte population, with a proposed designation of P3, that appeared circulating in the CF on day 7 p.a. and was more abundant on day 14 p.a. P3 cells showed similar morphologic values to the P1 population, however with similar fluorescence values to P2. Histology showed continuous progress of the RNC regeneration. The first reaction is a behavioral defense, in which the tube feet are retracted, where the nerve tissue was amputated, to protect the wound. Consequently, the tube feet lose their motor function, and the sea star stops using this arm as the movement leader (data not published). On day 1 p.a. the ends of the RNC are already sealed and healed. The migration of molecules and/or cells through the CF is evident since the WVC and the HS display slight hypertrophy. On day 7 p.a. an early regeneration phase is already happening, and the hypertrophy of the coelomic canals is more accentuated. Moreover, the RNC ends are connected by nerve tissue consisting of the hyaline layer, the somatic zone, a thin/absence of the neuropile, and the hyponeural epithelia. Finally, on day 14 p.a., the regenerative zone of the nerve resembles in structure and composition the normal zone, being the RNC almost fully regenerated.

# 5. FUTURE PRESPECTIVES

Working with non-model organisms has its complexities and setbacks, where the optimization of protocols is a constant must do. As the experimentation on starfish is still in its infancy, future methodological techniques have to be continuously applied in order to increase the knowledge of the molecular pathways associated with several tissues and organs regarding the regenerative success observed in this organism. Regarding the regeneration study of the RNC, LC-MS/MS quantitative and qualitative analysis of CFF proteins would contribute to the clarification of the cellular and molecular processes involved in these events. Also, since CE is a neighbor tissue in direct contact with the CF and suggested to have a potential hematopoietic role, these methods coupled with proteomics regarding the CE of the coelomic cavity would be the next step to build a more complete characterization of the RNC regeneration. In order to move forward, it would be also valuable to perform metabolomic and transcriptomic analysis of the RNC tissue. However, keeping in mind that the nerve tissue probably is not the only tissue in regeneration, due to difficulties in handling the regeneration induction of the RNC. Here it was evident that the total protein quantity in the CFF of starfish is very low, so to do LC-MS/MS analysis is suggested to pool proteins extracts from several individuals (of at least three animals to comply with the minimum quantity of CFF protein required). Finally, the characterization of this new P3 cell population resorting to IFC is a must do, in order to visualize real images of these cells, and to characterize them through fluorescence and morphologic parameters. For a more complete characterization of this population, is advised to study its cell cycle and ploidy through FC.

# 6. REFERENCES


[1] Díaz-Balzac, C. A., & García-Arrarás, J. E. (2018). Echinoderm Nervous System. *Oxford Research Encyclopedia of Neuroscience*. https://doi.org/10.1093/acrefore/9780190264086.013.205.

[2] Smith, L. C., Ari, V., Hudgell, M. A. B., Barone, G., Bodnar, A. G., Buckley, K. M., Cunsolo, V., Dheilly, N. M., Franchi, N., Fugmann, S. D., Furukawa, R., Arraras, J. G.-, Henson, J. H., Hibino, T., Irons, Z. H., Li, C., Lun, C. M., Majeske, A. J., Oren, M., Pagliara, P., Pinsino, A., Raftos, D. A., Rast, J. P., Samasa, B., Schillaci, D., Schrankel, C. S., Stabili, L., Stensvag, K., & Sutton, E. (2018). *Echinodermata: The Complex Immune System in Echinoderms*. https://doi.org/10.1007/978-3-319-76768-0.

[3] Garcia-Arraras, J., & Dolmatov, I. (2010). Echinoderms: Potential Model Systems for Studies on Muscle Regeneration. *Current Pharmaceutical Design*, *16*(8), 942–955. https://doi.org/10.2174/138161210790883426.

[4] Franco, F. (2011). *Proteomics based approach to understand tissue regeneration* [Doctoral dissertation, Instituto de Tecnologia Química e Biológica]. Universidade Nova de Lisboa repository. http://hdl.handle.net/10362/14118

[5] Ruppert, E. E., Fox, R. S., Barnes, R. D. (2004). *Invertebrate zoology: a functional evolutionary approach* (7th ed.). Belmont, CA: Thomson-Brooks/Cole.

[6] Mashanov, V., Zueva, O., Mashanov, V., Mashanov, V., Zueva, O., Rubilar, T., Epherra, L., & García-arrarás, J. E. (2016). Echinodermata. In *Structure and Evolution of Invertebrate Nervous Systems (Chapter 51)*. Oxford University Press. https://DOI:10.1093/acprof:oso/9780199682201.001.0001.

[7] Mashanov, V., & Zueva, O. (2020). Radial Glia in Echinoderms. *HHS Public Access*, *79*(5), 396–405. https://doi.org/10.1002/dneu.22659.Radial.

[8] Blowes, L. M., Egertová, M., Liu, Y., Davis, G. R., Terrill, N. J., Gupta, H. S., & Elphick, M. R. (2017). Body wall structure in the starfish *Asterias rubens*. *Journal of Anatomy*, *231*(3), 325–341. https://doi.org/10.1111/joa.12646.

[9] Ferguson, J. C. (1984). Translocative Functions of the Enigmatic Organs of Starfish: The Axial Organ, Hemal Vessels, Tiedemann's Bodies, and Rectal Caeca: An Autoradiographic Study. *The Biological Bulletin, 166*(1), 98-110.

[10] Daviddi, A. (2014). *Microscopic anatomy of arm-tip regeneration in the starfish Marthasterias glacialis (Linneaus, 1758) following traumatic amputation* [Master dissertation, Facoltà di Scienze e Tecnologie, Universtità Degli Studi di Milano]. ResearchGate. https://www.researchgate.net/publication/321906663_Microscopic_anatomy_of_arm-tip_regeneration_in_the_starfish_Marthasterias_glacialis_Linneaus_1758_following_traumatic_amputation

[11] Mashanov, V. S., Zueva, O. R., & García-Arrarás, J. E. (2013). Radial glial cells play a key role in echinoderm neural regeneration. *BMC Biology*, *11*(49). https://doi.org/10.1186/1741-7007-11-49.

[12] Ortega, A., & Olivares-Bañuelos, T. N. (2020). Neurons and Glia Cells in Marine Invertebrates: An Update. *Frontiers in Neuroscience*, *14*, 1–14. https://doi.org/10.3389/fnins.2020.00121.

[13] Franco, C. F., Santos, R., & Coelho, A. V. (2011). Exploring the proteome of an echinoderm nervous system: 2-DE of the sea star radial nerve cord and the synaptosomal membranes subproteome. *Proteomics*, *11*(7), 1359–1364. https://doi.org/10.1002/pmic.201000541.

[14] Pinsino, A., Thorndyke, M. C., & Matranga, V. (2007). Coelomocytes and Post-Traumatic Response in the common sea star *Asterias rubens*. *Cell Stress & Chaperones*, *12*(4), 331–341. https://doi:10.1379/CSC-288.1.

[15] Smith, L. C., Dheilly, N., Smith, L. C., Ghosh, J., Buckley, K. M., Clow, L. A., Dheilly, N. M., Haug, T., Henson, J. H., Li, C., Lun, C. M., Majeske, A. J., Matranga, V., Nair, S. V, Rast, J. P., Raftos, D. A., Roth, M., Sacchi, S., Schrankel, C. S., & Stensvåg, K. (2010). Echinoderm Imunnity. *Invertebrate Imunnity, Landes Bioscience and Springer Science+Business Media*, *14*, 260-301.

[16] Shabelnikov, S., Bobkov, D. E., Sharlaimova, N. S., & Petukhova, O. (2019). Injury affects coelomic fluid proteome of the common starfish, *Asterias rubens*. *Journal of Experimental Biology*, *222*(6). https://doi.org/10.1242/jeb.198556.

[17] Chiaramonte, M., & Russo, R. (2015). The echinoderm innate humoral immune response. *Italian Journal of Zoology*, *82*(3), 300–308. https://doi.org/10.1080/11250003.2015.1061615.

[18] Ramírez-Gómez, F. J., & García-Arrarás, J. E. (2010). Echinoderm immunity. *Information Systems Journal*, *7*, 211-220.

[19] Franco, C. F., Santos, R., & Coelho, A. V. (2011). Proteome characterization of sea star coelomocytes – The innate immune effector cells of echinoderms. *Protoeomics*, *11*, 3587–3592. https://doi.org/10.1002/pmic.201000745.

[20] Verling, E., Crook, A., & Harrison, S. (2003). Structural dynamics of a sea-star (*Marthasterias glacialis*) population. *Journal of the Marine Biological Association of the UK*, *83*(3), 583-592. https://doi.org/10.1017/S0025315403007513h.

[21] Tuya, F., & Duarte, P. (2012). Efecto de la disponibilidad alimenticia sobre la distribución batimétrica de la estrella de mar *Marthasterias glacialis* (Lamk.) en arrecifes del norte de Portugal. *Scientia Marina*, *76*(1), 9–15. https://doi.org/10.3989/scimar.2012.76n1009.

[22] Sodergren, E. (2006). The Genome of the Sea Urchin *Strongylocentrotus purpuratus*. *Science*, *314*(5801), 941-952. https://doi.org/10.1126/science.1133609.

[23] Khadra, Y. Ben, Sugni, M., Ferrario, C., Bonasoro, F., Coelho, A. V., Martinez, P., Daniela, M., & Carnevali, C. (2017). An integrated view of asteroid regeneration: tissues, cells and molecules. *Cell and Tissue Research*, *370*, 13–28. https://doi.org/10.1007/s00441-017-2589-9.

[24] Candia-carnevali, M. D., Thorndyke, M. C., & Matranga, V. (2009). Regenerating Echinoderms: A Promise to Understand Stem Cells Potential. *Stem Cell in Marine Organisms*, 165–186. https://doi.org/10.1007/978-90-481-2767-2.

[25] Ku, H. S., & Burghardt, T. (2013). Animal biometrics: quantifying and detecting phenotypic appearance. *Cell Press*, *28*(7), 432-441. https://doi.org/10.1016/j.tree.2013.02.013.

[26] Laires, S. (2012). *Characterization of the coelomic fluid of the starfish Marthasterias glacialis in a wound-healing phase* [Master dissertation, Instituto Superior Técnico]. Universidade de Lisboa repository.

[27] Oliveira, B. (2016). *Dynamics of circulating coelomocytes during starfish regeneration* [Master dissertation, Faculdade de Ciências]. Universidade de Lisboa repository. http://hdl.handle.net/10451/25862

[28] Bernstein, B. B., Williams, B. M., & Mann, K. H. (1981). The role of behavioral responses to predators in modifying urchins' (*Strongylocentrotus droebachiensis*) destructive grazing and seasonal foraging patterns. *Marine Biology 63*, 39–49. https://doi.org/10.1007/BF00394661.

[29] Temara, A., Gulec, I., & Holdway, D. A. (1999). Oil-induced disruption of foraging behaviour of the asteroid keystone predator, *Coscinasterias muricata* (Echinodermata). *Marine Biology*, 133:501-507.

[30] Di Trapani, F., Gianguzza, P., Galasso, N., & Riggio, S. (2013). Biometric Relationships in *Marthasterias Glacialis* (L.) (Asteroidea). *Biologia Marina Mediterranea*, *20*(1), 132–133.

[31] Barker, M.F., & Nichols, D. (1983). Reproduction, recruitment and juvenile ecology of the starfish, *Asterias rubens* and *Marthasterias glacialis*. *Journal of the Marine Biological Association of the United Kingdom*, *63*, 745-765.

[32] Gaymer, C. F., & Himmelman, J. H. (2002). Mussel beds in deeper water provide an unusual situation for competitive interactions between the seastars *Leptasterias polaris* and *Asterias vulgaris*. *Journal of Experimental Marine Biology and Ecology*, *277*, 13–24.

[33] Gaymer, C. F., & Himmelman, J. H. (2008). A keystone predatory sea star in the intertidal zone is controlled by a higher-order predatory sea star in the subtidal zone. *Marine Ecology Progress Series*, *370*, 143–153. https://doi.org/10.3354/meps07663.

[34] Penney, A. J., & Griffiths, C. L. (1984). Prey selection and the impact of the starfish *Marthasterias glacialis* (L.) and other predators on the mussel *Choromytilus meridionalis* (Krauss). *Journal of Experimental Marine Biology and Ecology*, 75, 19-36.

[35] Frid, C. L. J. (1992). Foraging behaviour of the spiny starfish *Marthasterias glacialis* in lough Ine, Co. Cork. *Marine Behaviour and Physiology*, *19*(4), 227– 239. https://doi.org/10.1080/10236249209378811.

[36] Ganmanee, M., Narita, T., Iida, S., & Sekiguchi, H. (2003). *Feeding habits of asteroids, Luidia quinaria and Astropecten scoparius. Fisheries Science*, 69:1121–1134.

[37] Minchin, D. (1987). Sea-water temperature and spawning behavior in the seastar *Marthasterias glacialis*. *Marine Biology*, *95*, 139-143.

[38] Scheibling, R. E., & Lauzon-Guay, J. S. (2007). Feeding aggregations of sea stars (*Asterias spp.* and *Henricia sanguinolenta*) associated with sea urchin (*Strongylocentrotus droebachiensis*) grazing fronts in Nova Scotia. *Marine Biology*, *151*(3), 1175–1183. https://doi.org/10.1007/s00227-006-0562-3.

[39] Urriago, J. D., Himmelman, J. H., & Gaymer, C. F. (2011). Responses of the black sea urchin *Tetrapygus niger* to its sea-star predators *Heliaster helianthus* and *Meyenaster gelatinosus* under field conditions. *Journal of Experimental Marine Biology and Ecology*, *399*(1), 17–24. https://doi.org/10.1016/j.jembe.2011.01.004.

[40] Wahltinez, S. J., & Stacy, N. I. (2020). Coelomic Fluid Evaluation in *Pisaster ochraceus* Affected by Sea Star Wasting Syndrome: Evidence of Osmodysregulation, Calcium Homeostasis Derangement, and Coelomocyte Responses. *Frontiers Veterinary Science*, *7*, 1–10. https://doi.org/10.3389/fvets.2020.00131.

[41] Sommer, U., Meusel B., & Stielau, C. (1999). An experimental analysis of the importance of body-size in the sea star-mussel predator-prey relationship. *Acta Oecologica*, *20*(2):81-86.

[42] Campbell, A. C., Mary, Q., Coppard, S. E., Abreo, C. D., & Mary, Q. (2001). Escape and Aggregation Responses of Three Echinoderms to Conspecific Stimuli. *The University Chicago Press*, *201*(2), 182-190. https://doi.org/10.2307/1543332.

[43] Gianguzza, P., di Trapani, F., Bonaviri, C., Visconti, G., Deidun, A., & Badalamenti, F. (2015). New body metrics to determine asteroid size and weight directly in the field. *Thalassas*, *31*(1), 73–82.

[44] Cai, W., Kim, C., Go, H., & Egertová, M. (2018). Biochemical, Anatomical, and Pharmacological Characterization of Calcitonin-Type Neuropeptides in Starfish: Discovery of an Ancient Role as Muscle Relaxants. *Frontiers in Neurosciences*, *12*, 1–24. https://doi.org/10.3389/fnins.2018.00382.

[45] Andrade, C., Oliveira, B., Guatelli, S., Martinez, P., Simões, B., Bispo, C., Ferrario, C., Bonasoro, F., Rino, J., Sugni, M., Gardner, R., Zilhão, R., Coelho, A. V. (2021). Characterization of Coelomic Fluid Cell Types in the Starfish *Marthasterias glacialis* Using a Flow Cytometry / Imaging Combined Approach. *Frontiers in Immunology*, *12*, 1–14. https://doi.org/10.3389/fimmu.2021.641664.

[46] Carnevali, C. (2006). Regeneration in Echinoderms: repair, regrowth, cloning. *Invertebrate Survival Journal*, *3*, 64–76.

[47] Khadra, Y. Ben, Sugni, M., Ferrario, C., Bonasoro, F., Oliveri, P., Martinez, P., Daniela, M., & Carnevali, C. (2018). Regeneration in Stellate Echinoderms: Crinoidea, Asteroidea and Ophiuroidea. In *Marine Organisms as Models Systems in Biology and Medicine* (pp. 285-320). https://doi:10.1007/978-3-319-92486-1_14.

[48] Ferrario, C., Sugni, M., Somorjai, I. M. L., Ballarin, L., & Burke, R. D. (2020). Beyond Adult Stem Cells: Dedifferentiation as a Unifying Mechanism Underlying Regeneration in Invertebrate Deuterostomes. *Frontiers in Cell and Development Biology*, *8*. https://doi.org/10.3389/fcell.2020.587320.

[49] Alvarado, A. S., & Tsonis, P. A. (2006). Bridging the regeneration gap: genetic insights from diverse animal models. *Nature Review Genetics*, *7*, 873–884. https://doi.org/10.1038/nrg1923.

[50] Agata, K., Saito, Y., & Nakajima, E. (2007). Unifying principles of regeneration I: Epimorphosis versus morphallaxis. *Development Growth and Differentiation*, *49*(2), 73–78. https://doi.org/10.1111/j.1440-169X.2007.00919.x.

[51] Brockes, J. (1997). Amphibian Limb Regeneration: Rebuilding a Complex Structure. *Science*, *276*(5309), 81-87. https://DOI:10.1126/science.276.5309.81.

[52] Suzuki, M., Yakushiji, N., Nakada, Y., Satoh, A., Ide, H., & Tamura, K. (2006). Limb regeneration in *Xenopus laevis* froglet. *The Scientific World Journal*, *6*, 26–37. https://doi.org/10.1100/tsw.2006.325.

[53] Franco, C. F., Soares, R., Pires, E., Santos, R., & Coelho, A. V. (2012). Radial nerve cord protein phosphorylation dynamics during starfish arm tip wound. *Electrophoresis*, *33*, 3764–3778. https://doi.org/10.1002/elps.201200274.

[54] Mashanov, V. S., Zueva, O. R., & García-arrarás, J. E. (2015). Heterogeneous generation of new cells in the adult echinoderm nervous system. *Frontiers in Neuroanatomy*, *9*, 1–13. https://doi.org/10.3389/fnana.2015.00123.

[55] Khahdra, Y. Ben, Said, K., & Thorndyke, M. (2014). Regeneration. *Biochemical Genetics*, *52*, 166–180. https://doi.org/10.1007/s10528-013-9637-2.

[56] Thorndyke, M. C., & Carnevali, M. D. C. (2001). Regeneration neurohormones and growth factors in echinoderms. *Canadian Journal of Zoology*, *79*(7), 1171–1208. https://doi.org/10.1139/cjz-79-7-1171.

[57] Ferraz Franco, C., Santos, R., & Varela Coelho, A. (2014). Proteolytic events are relevant cellular responses during nervous system regeneration of the starfish *Marthasterias glacialis*. *Journal of Proteomics*, *99*, 1–25. https://doi.org/10.1016/j.jprot.2013.12.012.

[58] Candia-Carnevali, M.D., & Burighel, P. (2010). Regeneration in Echinoderms and Ascidians. *Encyclopedia of Life Sciences*. https://doi.org/10.1002/9780470015902.a0022102.

[59] Smith, P. K., Krohn, R. I., Hermanson, G. T., Mallia, A. K., Gartner, F. H., Provenzano, M. D., Fujimoto, E. K., Goeke, N. M., Olson, B. J., & Klenk, D. C. (1985). Measurement of Protein Using Bicinchoninic Acid. *Analytical Biochemistry*, *150*(1), 76-85. https://doi:10.1016/0003-2697(85)90442-7.

[60] Milligan, M. (1946). Trichrome stain for formalin-fixed tissue. *American Journal of Clinical Pathology, Technical Section*, *10*(6), 184-185. https://doi:10.1093/ajcp/16.11_ts.184.

[61] Mah, C.L., & Blake, D.B. (2012). Global Diversity and Phylogeny of the Asteroidea (Echinodermata). *PLOS ONE*, *7*(4), 35644. https://doi:10.1371/journal.pone.0035644.

[62] Forsman, A., & Wennersten, L. (2016). Inter-individual variation promotes ecological success of populations and species: evidence from experimental and comparative studies. *Ecography*, *39*(7), 630–648. https://doi.org/10.1111/ecog.01357.

[63] Bay-Nouailhat, A. (2005). Description of Marthasterias glacialis. Accessed in November 2020. Available from: http://www.european-marine-life.org/30/marthasterias-glacialis.php

[64] Ager, O.E.D. (2008). Marthasterias glacialis Spiny starfish. Accessed in November 2020. Available from: https://www.marlin.ac.uk/species/detail/1688.

[65] Sköld, M., Barker, & M., Mladenov, P. (2002). Spatial variability in sexual and asexual reproduction of the fissiparous seastar *Coscinasterias muricata*: the role of food and fluctuating temperature. *Marine Ecology Progress Series*, *233*, 143-155. https://doi:10.3354/meps233143.

[66] Rubilar, T., Meretta, P.E., & Cledón, M. (2014). Regeneration rate after fission in the fissiparous sea star *Allostichaster capensis* (Asteroidea). *Revista de Biología Tropical*, *63*(2), 321-328. http://dx.doi.org/10.15517/rbt.v63i2.23166.

[67] Ohsima, H., and Ikeda, H. (1934). Sexual size-dimorphism in the sea star *Archaster typicus* Mull. et Trosh. *Proceedings of the Imperial Academy*, *10*(3), 180-183. https://doi.org/10.2183/pjab1912.10.180.

[68] Olsen, B.J., & Markwell, J. (2007). Assays for the Determination of Protein Concentration. *Current Protocols in Protein Science*, *48*, 14–17. https://doi.org/10.1002/0471140864.ps0304s48.

[69] Matozzo, V., & Marin, M. G. (2010). First evidence of gender-related differences in immune parameters of the clam Ruditapes philippinarum (Mollusca, Bivalvia). *Marine Biology*, 157(6), 1181–1189. https://doi:10.1007/s00227-010-1398-4.

[70] Grilo, T. F., Lopes, A. R., Sampaio, E., Rosa, R., & Cardoso, P. G. (2018). Sex differences in oxidative stress responses of tropical topshells (*Trochus histrio*) to increased temperature and high p CO 2. *Marine Pollution Bulletin*, *131*, 252–259. https://doi:10.1016/j.marpolbul.2018.04.0.

[71] Arizza, V., Vazzana, M., Schillaci, D., Russo, D., Giaramita, F. T., & Parrinello, N. (2013). Gender differences in the immune system activities of sea urchin *Paracentrotus lividus*. *Comparative Biochemistry and Physiology Part A: Molecular & Integrative Physiology*, *164*(3), 447–455. https://doi:10.1016/j.cbpa.2012.11.021.

[72] Jiang, J., Zhou, Z., Dong, Y., Gao, S., Sun, H., Chen, Z., Yang, A., & Su, H. (2017). Comparative analysis of immunocompetence between females and males in the sea cucumber *Apostichopus japonicus*. *Fish and Shellfish Immunology*, *63*, 438–443. https://doi.org/10.1016/j.fsi.2017.02.038.

[73] Jiang, J., Zhao, Z., Pan, Y., Dong, Y., Gao, S., Li, S., Wang, C., Yang, H., Lin, S., & Zhou, Z. (2019). Gender specific differences of immune competence in the sea cucumber *Apostichopus japonicus* before and after spawning. *Fish and Shellfish Immunology*, *90*, 73–79. https://doi.org/10.1016/j.fsi.2019.04.051.

[74] Jiang, J., Zhao, Z., Pan, Y., Dong, Y., Gao, S., Jiang, B., Xiao, Y., Jiang, P., Zhang, G., Wang, X., & Zhou, Z. (2020). Proteomics reveals the gender differences in humoral immunity and physiological characteristics associated with reproduction in the sea cucumber *Apostichopus japonicus*. *Journal of Proteomics*, *217*, 1874-3919. https://doi.org/10.1016/j.jprot.2020.103687.

[75] Canicatti, C. (1989). Evolution of the lytic system in echinoderms—II. Naturally occurring hemolytic activity in *Marthasterias glacialis* (Asteroidea) coelomic fluid. *Comparative Biochemistry and Physiology Part A: Physiology*, *93*(3), 587–591. https://doi:10.1016/0300-9629(89)90015-7.

[76] Sharlaimova, N., Shabelnikov, S., & Petukhova, O. (2014). Small coelomic epithelial cells of the starfish *Asterias rubens L*. that are able to proliferate in vivo and in vitro. *Cell and Tissue Research*, *356*(1), 83–95. https://doi.org/10.1007/s00441-013-1766-8.

[77] Park, Y., Abihssira-García, I. S., Thalmann, S., Wiegertjes, G. F., Barreda, D. R., Olsvik, P. A., & Kiron, V. (2020). Imaging Flow Cytometry Protocols for Examining Phagocytosis of Microplastics and Bioparticles by Immune Cells of Aquatic Animals. *Frontiers in Immunology*, *11*, 203. https://doi.org/10.3389/fimmu.2020.00203.

[78] Ogle, L. F., Orr, J. G., Willoughby, C. E., Hutton, C., McPherson, S., Plummer, R., Boddy, A. v., Curtin, N. J., Jamieson, D., & Reeves, H. L. (2016). Imagestream detection and characterisation of circulating tumour cells – A liquid biopsy for hepatocellular carcinoma? *Journal of Hepatology*, *65*(2), 305–313. https://doi.org/10.1016/j.jhep.2016.04.014.

[79] Byrne, M. (2020). The Link between Autotomy and CNS Regeneration: Echinoderms as Non-Model Species for Regenerative Biology. *BioEssays*, *42*(3), 1900219. https://doi:10.1002/bies.201900219.

[80] Franco, C., Soares, R., Pires, E., Koci, K., Almeida, A. M., Santos, R., & Coelho, A. V. (2013). Understanding regeneration through proteomics. *Proteomics*, *13*, 686–709. https://doi.org/10.1002/pmic.201200397.

[81] Smith, P. J., Wiltshire, M., & Errington, R. J. (2004). DRAQ5 Labeling of Nuclear DNA in Live and Fixed Cells Nucleic Acid Analysis. *Current Protocols in Cytometry*, *7*. https://DOI:10.1002/0471142956.cy0725s28.

[82] Leclerc, M., & Bajelan, M. (1992). Homologous antigen for T cell receptor in axial organ cells from the asterid *Asterias rubens*. *Cell Biology International Reports*, *6*(5), 487-90. https://doi:10.1016/s0309-1651(06)80068-8.

[83] Kaneshiro, E. S., & Karp, R. D. (1980). The ultrastructure of coelomocytes of the sea star *Dermasterias imbricata*. *The Biological Bulletin*, *159*(2), 295-310.

[84] Ferguson, J. C. (1966). Cell Production in the Tiedemann Bodies and Haemal Organs of the Starfish, *Asterias forbesi*. *Transactions of the American Microscopical Society*, *85*(2), 200-209.

[85] Sharlaimova, N., Shabelnikov, S., Bobkov, D., Martynova, M., Bystrova, O., & Petukhova, O. (2021). Coelomocyte replenishment in adult *Asterias rubens*: the possible ways. *Cell and Tissue Research*, *383*(3), 1043–1060. https://doi.org/10.1007/s00441-020-03337-z.

[86] Holm, K., Dupont, S., Sköld, H., Stenius, A., Thorndyke, M., & Hernroth, B. (2008). Induced cell proliferation in putative haematopoietic tissues of the sea star, *Asterias rubens* (L.). *Journal of Experimental Biology*, *211*(16), 2551–2558. https://doi.org/10.1242/jeb.018507.

[87] Bossche, J.P.V., & Jangoux, M. (1976). Epithelial origin of starfish coelomocytes. *Nature*, *261*(5557), 227–228. https://doi.10.1038/261227a0.

[88] Hernroth, B., Farahani, F., Brunborg, G., Dupont, S., Dejmek, A., & Sköld, H. N. (2010). Possibility of mixed progenitor cells in sea star arm regeneration. *Journal of Experimental Zoology Part B: Molecular and Developmental Evolution*, *314*(6), 457–468. https://doi.org/10.1002/jez.b.21352.

[89] Ben Khadra, Y., Ferrario, C., Benedetto, C. D., Said, K., Bonasoro, F., Candia Carnevali, M. D., & Sugni, M. (2015). Re-growth, morphogenesis, and differentiation during starfish arm regeneration. *Wound Repair and Regeneration*, 23(4), 623–634. https://doi:10.1111/wrr.12336.

[90] San Miguel-Ruiz, J. E., Maldonado-Soto, A. R., & García-Arrarás, J. E. (2009). Regeneration of the radial nerve cord in the sea cucumber *Holothuria glaberrima*. *BMC Developmental Biology*, *9*(1). https://doi.org/10.1186/1471-213X-9-3.

[91] Mashanov, V. S., Zueva, O. R., & García-Arrarás, J. E. (2017). Inhibition of cell proliferation does not slow down echinoderm neural regeneration. *Frontiers in Zoology*, *14*(1). https://doi.org/10.1186/s12983-017-0196-y.

[92] Ben Khadra, Y., Ferrario, C., di Benedetto, C., Said, K., Bonasoro, F., Candia Carnevali, M. D., & Sugni, M. (2015b). Wound repair during arm regeneration in the red starfish *Echinaster sepositus*. *Wound Repair and Regeneration*, *23*(4), 611–622. https://doi.org/10.1111/wrr.12333.

[93] Moss, C., Jackie Hunter, A., & Thorndyke, M. C. (1998). Patterns of bromodeoxyuridine incorporation and neuropeptide immunoreactivity during arm regeneration in the starfish *Asterias rubens*. *Philosophical Transactions of the Royal Society B: Biological Sciences*, 353(1367), 421–436. https://doi.org/10.1098/rstb.1998.0220.

[94] Ferrario, C. (2013). Arm-tip regeneration in the red starfish *Echinaster sepositus* (Echindermata, Asteroidea) following traumatic amputation: morphological and ultrastructural analyses [Masther dissertation, Facoltà di Scienze e Tecnologie]. Universitá Degli Studi di Milano repository. https://air.unimi.it/handle/2434/524592

[95] Guatelli, S. (2017). Coelomic epithelium and coelomocytes of *Marthasterias glacialis* (Asteroidea) in normal and regenerating arm-tips: microscopic anatomy and proteomics characterization [Masther dissertation, Facoltà di Scienze e Tecnologie]. Research Gate. https://www.researchgate.net/publication/320395183_Coelomic_epithelium_and_coelomocytes_of_Marthasterias_glacialis_Asteroidea_in_normal_and_regenerating_arm-tips_microscopy_anatomy_and_proteomics_characterization.

# ATTACHMENTS

Attachment 1. Starfish images
https://drive.google.com/drive/folders/1R0IpnurDnt8FTw-l7woLeuv5KGdTfMRY?usp=sharing.

Attachment 2. Determination of CFF total protein quantification
https://docs.google.com/document/d/1_0ez8WBlvg-yeqWpJCCtL8_E4p4hsa0b/edit?usp=sharing&ouid=114121496259295680385&rtpof=true&sd=true.

Attachment 3. Overall data- here is displayed three different data sets. In the first page, called Biometric Data, appears all the biometric parameters measured in the starfish, and the specimen's gender. In the second page, called CFF Total Protein, appears the data determined through the BCA assay for the non-regenerative samples, the corresponding harvest date of the CF and gender. The third page, called Nerve Regeneration Results, is present data determined through the BCA assay and FC for the regenerative studies.
https://docs.google.com/spreadsheets/d/1tITWr2EzQlXKWPHZV_X32wd48X9WQOj5/edit?usp=sharing&ouid=114121496259295680385&rtpof=true&sd=true.